

 Open access • Posted Content • DOI:10.1101/2021.06.18.448918

RPAP2 regulates a transcription initiation checkpoint by prohibiting assembly of preinitiation complex — [Source link](#)

Xueping Chen, Xueping Chen, Yilun Qi, Xiangdong Wang ...+10 more authors

Institutions: Fudan University Shanghai Medical College, Fudan University, Chinese Academy of Sciences

Published on: 18 Jun 2021 - bioRxiv (Cold Spring Harbor Laboratory)

Topics: Transcription factor II F, RNA polymerase II, Transcription preinitiation complex, Transcription (biology) and RNA polymerase

Related papers:

- [A TBP-independent mechanism for RNA Polymerase II transcription](#)
- [Transcriptional Regulation by Pol II\(G\) Involving Mediator and Competitive Interactions of Gdown1 and TFIIIF with Pol II](#)
- [Structures of mammalian RNA polymerase II pre-initiation complexes](#)
- [Biochemical analysis of transcription termination by RNA polymerase III from yeast *Saccharomyces cerevisiae*.](#)
- [Structure and mechanism of the RNA polymerase II transcription machinery.](#)

Share this paper:    

View more about this paper here: <https://typeset.io/papers/rpap2-regulates-a-transcription-initiation-checkpoint-by-292nwagi6>

24 **Abstract**

25 RNA polymerase II (Pol II)-mediated transcription in metazoan requires precise regulation.
26 RNA polymerase II-associated protein 2 (RPAP2) was previously identified to transport Pol II
27 from cytoplasm to nucleus and dephosphorylates Pol II C-terminal domain (CTD). We found
28 that RPAP2 binds hypo/hyper-phosphorylated Pol II with undetectable phosphatase activity.
29 Structure of RPAP2-Pol II shows mutually exclusive assembly of RPAP2-Pol II and pre-
30 initiation complex (PIC) due to three steric clashes. RPAP2 prevents/disrupts Pol II-TFIIF
31 interaction and impairs in vitro transcription initiation, suggesting a function in prohibiting PIC
32 assembly. Loss of RPAP2 in cells leads to global accumulation of TFIIF and Pol II at promoters,
33 indicating critical role of RPAP2 in inhibiting PIC assembly independent of its putative
34 phosphatase activity. Our study indicates that RPAP2 functions as a gatekeeper to prohibit PIC
35 assembly and transcription initiation and suggests a novel transcription checkpoint.

36 Introduction

37 The sequence-specific transcription factors (TFs) bind regulatory elements (promoters and
38 enhancers) and multi-subunit Mediator to facilitate the assembly of a preinitiation complex
39 (PIC) and activate RNA polymerase II (Pol II)-mediated eukaryotic transcription initiation on
40 target genes. PIC assembly involves sequential recruitment of general transcription factors
41 (GTFs) TFIID, TFIIA, TFIIB, TFIIF-bound Pol II, TFIIE, and TFIIH ([Roeder, 1996](#); [Thomas
42 and Chiang, 2006](#); [Zawel and Reinberg, 1993](#)). Within the 10-subunit TFIIH, the DNA
43 translocase subunit (XPB) stimulates promoter opening ([Guzder et al., 1994](#); [Lin et al., 2005](#))
44 and the cyclin-dependent kinase 7 (CDK7) phosphorylates Ser5 residues of the heptapeptide
45 repeats (Y¹S²P³T⁴S⁵P⁶S⁷) of the RPB1 C-terminal domain (CTD) ([Feaver et al., 1994](#); [Fisher
46 and Morgan, 1994](#)), the two processes required for transcription initiation. As a focal point of
47 transcription regulation, activation of transcription initiation has been well-characterized
48 through biochemical studies ([Buratowski et al., 1989](#); [Cortes et al., 1992](#); [Flores et al., 1991](#))
49 and was recently revealed by structural studies from our group and others ([Abdella et al., 2021](#);
50 [Chen et al., 2021a](#); [Chen et al., 2021b](#); [Rengachari et al., 2021](#)). Compared to extensive studies
51 of positive regulation, negative regulation of transcription initiation is less understood.

52 The human RNA polymerase II-associated protein 2 (RPAP2) and its yeast homolog regulator
53 of transcription protein (Rtr1) were originally identified to transport the associated Pol II from
54 the cytoplasm to nucleus ([Forget et al., 2013](#); [Gibney et al., 2008](#)). Cytoplasm accumulation of
55 RPAP2 was observed in Myofibrillar myopathies, a group of neuromuscular disorders
56 ([Guglielmi et al., 2015](#)). Subsequent studies showed that depletion of RPAP2/Rtr1 led to defect
57 of transcription termination ([Victorino et al., 2020](#)) and increase in the level of Ser5-
58 phosphorylation (pSer5) of Pol II CTD ([Egloff et al., 2012](#); [Hunter et al., 2016](#); [Kim et al.,
59 2009](#); [Mosley et al., 2009](#)), which serves as an indicator of enhanced transcription initiation.
60 As RPAP2-binding partners, regulator of pre-mRNA-domain-containing 1A (RPRD1A) and
61 RPRD1B form heterodimer and preferentially bind Pol II with CTD phosphorylated at
62 Ser2/Ser7 ([Ni et al., 2014](#)) and acetylated at position 7 lysine residues ([Ali et al., 2019](#)),
63 consistent with the interaction between hyperphosphorylated Pol II and Rtr1 ([Smith-Kinnaman
64 et al., 2014](#)).

65 The role of RPAP2/Rtr1 in transcription regulation has been believed to be derived from the
66 phosphatase activity of RPAP2 ([Egloff et al., 2012](#)) and Rtr1 ([Mosley et al., 2009](#)). However,
67 in vitro biochemical analyses ([Hsu et al., 2014](#); [Xiang et al., 2012](#)) indicated the RPAP2/Rtr1
68 possesses undetectable phosphatase activity or much lower activity compared to other known
69 Pol II CTD phosphatases, such as Ssu72 ([Zhang et al., 2011](#)), Scp1 ([Zhang et al., 2006](#)), and

70 Fcp1 ([Hausmann and Shuman, 2002](#)). Structural studies indicated that Rtr1 of *Kluyveromyces*
71 *lactis* and *Saccharomyces cerevisiae* adopt similar fold, which lacks well-defined catalytic
72 pocket of phosphatase ([Hsu et al., 2014](#); [Irani et al., 2016](#); [Xiang et al., 2012](#)). The lack of
73 efficient phosphatase activity suggests that RPAP2/Rtr1 may involve transcription regulation
74 through a phosphatase-independent function.

75 Here, we observed near stoichiometric association of endogenous RPAP2 during the
76 purification of recombinant human Pol II. The *in vitro* assay showed undetectable phosphatase
77 activity on phosphorylated Pol II CTD. The cryo-electron microscopy (EM) structures of
78 RPAP2-Pol II complexes indicate mutually exclusive assembly of RPAP2-Pol II with PIC or
79 elongation complex (EC). Biochemical analysis indicated that RPAP2 prevents Pol II-TFIIF
80 interaction, disrupts Pol II-TFIIF complex, and inhibits *in vitro* transcription initiation.
81 Chromatin immunoprecipitation (ChIP)-sequencing analysis showed that the deletion of
82 RPAP2 led to an increase of TFIIF occupancy on promoters, indicative of enhanced assembly
83 of PIC. Such negative effect on transcription initiation is independent of the putative
84 phosphatase activity of RPAP2. Thus, we identified a transcription pre-initiation checkpoint,
85 in which RPAP2 binds Pol II and prevents PIC assembly and transcription initiation.

86 **Results**

87 **RPAP2 binds Pol II but shows undetectable phosphatase activity**

88 During purification of human Pol II overexpressed in Expi293F cells, we observed a stably co-
89 purified Pol II-binding partner (Figure 1A). Mass spectrometry (MS) analysis indicated that
90 the protein is RNA polymerase II associated protein 2 (RPAP2), a previously identified Pol II-
91 binding protein. We observed higher and lower bands of RPB1 in the purified Pol II, indicative
92 of Pol II in the hyperphosphorylated (Pol II_o) and hypophosphorylated (Pol II_a) forms,
93 respectively. Consistently, trace amount of phosphorylated Pol II (phosphorylation of CTD at
94 Ser2, Ser5, and Ser7) could be detected from the purified RPAP2, which was overexpressed in
95 Expi293F cells (Figure 2E, lane 1). To test whether RPAP2 binds Pol II_a or Pol II_o, we next
96 separately purified RPAP2 and prepared phosphorylated Pol II as previously described ([Zheng
97 et al., 2020](#)) (Figures 1B and 2E). The in vitro pulldown assay showed that RPAP2 binds Pol
98 II in the two phosphorylation forms, indicating that Pol II CTD phosphorylation is not required
99 for RPAP2-Pol II interaction.

100 The human RPAP2 and its yeast homolog Rtr1 have been reported to possess protein
101 phosphatase activity against phosphorylated Ser5 (pSer5) of Pol II CTD ([Egloff et al., 2012](#);
102 [Hsu et al., 2014](#); [Kim et al., 2009](#); [Mosley et al., 2009](#)). However, RPAP2-bound Pol II
103 remained evidently hyperphosphorylated after the two-day purification (Figure 1A),
104 suggesting inefficient dephosphorylation of RPAP2 on phosphorylated Pol II CTD.

105 To directly measure RPAP2 phosphatase activity, we performed an in vitro phosphatase assay
106 using the phosphorylated Pol II as substrate, which possesses pSer5 and pSer2 of RPB1 CTD
107 (Figure 1C, lane 1). As a positive control, integrator-containing PP2A complex (INTAC) at 0.4
108 μM concentration showed largely dephosphorylated RPB1 (lane 2), consistent with our
109 previous study ([Zheng et al., 2020](#)). In contrast, RPAP2 at a concentration of as high as 10 μM
110 showed undetectable phosphatase activity (lanes 3 and 4), suggesting that RPAP2 possesses
111 very weak, if any, phosphatase activity against pSer5 of Pol II CTD. The result is consistent
112 with previous structural and biochemical studies showing that that Rtr1 (RPAP2 homolog)
113 lacks an active site and phosphatase activity ([Xiang et al., 2012](#)). Collectively, the in vitro
114 assays suggest that RPAP2 does not efficiently dephosphorylates Pol II CTD and Pol II CTD
115 phosphorylation is not required for binding of RPAP2 to Pol II, suggesting a phosphorylation
116 independent role of RPAP2 in Pol II function.

117

118 **Structure of RPAP2-Pol II complex**

119 We next determined the structure of human RPAP2-Pol II complex using cryo-EM single
120 particle reconstruction and the cryo-EM map was refined to 3.5 Å resolution (Figures S1 and
121 S2). RPRD1A-RPRD1B heterodimer was previously reported to bind RPAP2 and facilitate the
122 recognition of phosphorylated Pol II CTD ([Ni et al., 2014](#)). We have also complexed *Sus scrofa*
123 Pol II (four-residue substitution in human Pol II) with human RPAP2 and RPRD1A-RPRD1B
124 followed by gradient fixation (Grafix) (Figure S1) ([Kastner et al., 2008](#)) and the cryo-EM map
125 was refined to 2.8 Å resolution. The two cryo-EM maps showed almost identical conformation
126 and RPRD1A-RPRD1B was not observed, consistent with the binding of RPRD1A-RPRD1B
127 to the highly flexible Pol II CTD.

128 Structure determination was focused on RPAP2-Pol II-RPRD1A-RPRD1B (termed RPAP2-
129 Pol II for simplicity) and the structure will be discussed below (Figure 2 and Video S1). The
130 cryo-EM map around RPAP2 was locally refined to 3.4 Å resolution. For structural model
131 building, the structural templates of Pol II from holo PIC (hPIC) complex (PDB: 7EGB) ([Chen](#)
132 [et al., 2021a](#)) and yeast Rtr1 (PDB: 4FC8) ([Xiang et al., 2012](#)) were respectively docked into
133 the cryo-EM map, followed by manual adjustment (Figure S2 and Table S1).

134 The modeled RPAP2 consists of an N-terminal domain (NTD^{RPAP2}, residues 41-182) followed
135 by an extended loop (residues 183-203), which we termed TFIIF inhibitory region (TFIIFⁱ^{RPAP2},
136 described below) (Figure 2A-2D and Video S1). The C-terminal region (204-612) was invisible
137 in the cryo-EM map, consistent with the predicted flexibility. The NTD^{RPAP2} consists of a five-
138 helix bundle and a characteristic zinc finger. The zinc finger and a short helix stabilize the five-
139 helix bundle on two opposite ends. The overall fold of NTD^{RPAP2} is generally similar to that
140 of the reported structures of yeast Rtr1 ([Hsu et al., 2014](#); [Irani et al., 2016](#); [Xiang et al., 2012](#))
141 (Figure S3A).

142 In RPAP2-Pol II, Pol II adopts a similar conformation to that in PIC ([Chen et al., 2021a](#); [Chen](#)
143 [et al., 2021b](#)) and EC ([Bernecky et al., 2016](#)) (Figures 3A and S4A). The NTD^{RPAP2} is grasped
144 by the RPB5 jaw and RPB1 jaw (Figure 2D). The five-helix bundle binds the parallel helices
145 of the RPB5 jaw. A two-stranded β-sheet (residues 114-128) protrudes out of the five-helix
146 bundle and packs against the RPB1 jaw. The tip (residues 120-125) of the β-sheet inserts into
147 and stabilizes a flanking hairpin of RPB1 jaw, which was not previously modeled due to the
148 lack of stabilization ([Bernecky et al., 2016](#); [Chen et al., 2021a](#); [Chen et al., 2021b](#)). The
149 TFIIFⁱ^{RPAP2} packs against the lobe of RPB2, which contacts the charge helix of TFIIF (TFIIFα
150 subunit) in PIC/EC.

151

152 **The N-terminal region of RPAP2 is necessary and sufficient for binding of Pol II**

153 We next performed in vitro pulldown assay to test the interaction between RPAP2 and Pol II.
154 Reciprocal pulldown assay indicated that full-length RPAP2 and the N-terminal region
155 (residues 1-204) bound Pol II (Figures 2E, lanes 11-12 and S3A, lanes 18-19) whereas the C-
156 terminal region (residues 205-612) showed undetectable binding of Pol II (Figure 2E, lane 13
157 and S3A, lane 20). Double-mutation C100A-C105A and C136A-C140A largely decreased the
158 interaction (Figure 2E, lanes 14-15 and S3A, lane 21-22), indicating a critical role of the zinc-
159 finger in maintaining the overall fold of NTD^{RPAP2}. The deletion of the β -sheet (residues 114-
160 128) decreased the interaction (Figures 2E, lanes 16 and S3A, lane 23), consistent with its
161 position in bridging NTD^{RPAP2} and RPB1 jaw of Pol II.

162 It was reported that mutation Y105A of yeast Rtr1 (equivalent of Y127A in RPAP2) impairs
163 phosphatase activity ([Irani et al., 2016](#)). The RPAP2-Pol II interaction was not obviously
164 affected by the mutation Y127A (Figure 2E lane 18 and S3A, lane 25), suggesting a
165 phosphatase-independent function of RPAP2 in binding of Pol II. Thus, RPAP2^{Y127A} represents
166 a phosphatase-dead mutant that maintains RPAP2-Pol II interaction. Moreover, the deletion of
167 extended loop region (residues 175-204) has no obvious effect on RPAP2-Pol II interaction.

168

169 **Three steric clashes between RPAP2 and PIC/EC elements**

170 Comparison of RPAP2-Pol II structure with the structures of PIC ([Chen et al., 2021a](#)) and EC
171 ([Bernecky et al., 2016](#)) complexes shows that the Pol II-bound RPAP2 may generate three
172 steric clashes with structural elements of PIC or EC (Figures 3A, 3B and S4A). (1) The
173 NTD^{RPAP2} generates steric clash (Clash-I) with the Pol II clamp in PIC/EC (Figures 3A and
174 S4A), consistent with the absence of cryo-EM density of the clamp in RPAP2-Pol II
175 reconstruction (Figure 2B). (2) The NTD^{RPAP2} generates an apparent clash (Clash-II) with DNA
176 at the entry tunnel in PIC/EC, suggesting that binding of Pol II to RPAP2 and DNA are
177 mutually exclusive. (3) Superimposition of RPAP2-Pol II and PIC shows obvious overlaps
178 (Clash-III) of the TFIIF α charge helix and TFIIF^{RPAP2} (Figure 3B and Video S2). The above
179 structural analyses suggest that RPAP2 either inhibits PIC/EC assembly or dissociates from
180 Pol II during assembly of PIC/EC if not undergoing significant conformational changes.

181

182 **RPAP2 disrupts Pol II-TFIIF interaction and prohibits PIC assembly**

183 It is known that RPAP2 shuttles from the cytoplasm and nucleus with the associated Pol II
184 ([Forget et al., 2013](#); [Gibney et al., 2008](#)), suggesting that the Pol II-bound RPAP2 may function
185 prior to the assembly of Pol II into PIC complex. To test whether RPAP2 affects transcription

186 initiation, we performed in vitro transcription initiation assay using purified RPAP2, Pol II,
187 and general transcription factors (GTFs) including TFIID, TFIIA, TFIIB, TFIIE, TFIIF, and
188 TFIIH. As previously described ([Chen et al., 2021b](#)), Pol II and GTFs generated expected 50
189 nucleotide (nt) RNA products on *HDM2* promoter, indicating successful transcription initiation
190 (Figure 3C, lane 3). In contrast, the pre-assembled RPAP2-Pol II showed undetectable
191 transcription activity (Figure 3C, lane 2), indicating that RPAP2-bound Pol II does not support
192 transcript initiation.

193 We next investigated in which step RPAP2 inhibits transcription initiation. It has been well-
194 accepted that TFIIF is the first GTF that binds Pol II in step stepwise PIC assembly and that
195 PIC is unable to be assembled in the absence of TFIIF ([Cortes et al., 1992](#); [Flores et al., 1991](#)).
196 Competitive pulldown assay showed that TFIIF stably binds Pol II and the Pol II-TFIIF
197 complex is disrupted by the addition of RPAP2 (Figure 3D). Compared to standard Pol II-
198 TFIIF assembly, much less TFIIF was observed in the peak fractions of Pol II in glycerol
199 density gradient ultracentrifugation no matter whether TFIIF was added to the pre-assembled
200 RPAP2-Pol II or RPAP2 was added to the pre-assembled Pol II-TFIIF (Figure 3E-3H). These
201 results indicate that RPAP2 prohibits Pol II-TFIIF assembly and disrupts Pol II-TFIIF
202 interaction but not vice versa. Consistently, an increasing amount of RPAP2 inhibits in vitro
203 transcription initiation (Figure S4B).

204 We next performed a competitive binding assay to test whether other GTFs could disrupt
205 RPAP2-Pol II interaction (Figure S4C-S4F). The immobilized RPAP2 was first incubated with
206 Pol II followed by the addition of purified GTFs. The interaction between RPAP2 and Pol II
207 was not obviously disrupted by TFIID-TFIIA-promoter, TFIIB, TFIIE, TFIIF, or TFIIH, in line
208 with the architectural placement of RPAP2 on Pol II. The result is also consistent with the in
209 vitro transcription assay (Figures 3C and S4B), suggesting that PIC assembly is inhibited by
210 RPAP2 whereas RPAP2-Pol II interaction is not disrupted by GTFs in the in vitro system.

211

212 **RPAP2 regulates a pre-initiation checkpoint during cellular PIC assembly**

213 To examine whether RPAP2 suppresses TFIIF recruitment and thus prohibits PIC assembly in
214 cells, we depleted RPAP2 in human DLD-1 cells by shRNA (Figure 4A) and conducted ChIP
215 with reference exogenous genome (ChIP-Rx) of TFIIF. The chromatin occupancy of TFIIF
216 reflects dissociation of RPAP2 from Pol II and initial assembly of PIC complex on promoters.
217 Strikingly, as shown by example genes (Figures 4B and S5A) and metagene analysis (Figure
218 4C), RPAP2 depletion greatly enhanced the binding of TFIIF at promoters, in supportive of
219 the inhibitory role of RPAP2 in PIC assembly in cells. Consistently, the levels of Pol II

220 increased at promoters upon RPAP2 depletion (Figure 4B and 4D). Measurement of total and
221 elongating Pol II, represented by Pol II phosphorylated at Serine 2 of CTD, at gene bodies
222 revealed an activation of transcription elongation, likely resulting from the increase in PIC
223 assembly (Figure S5B-S5D).

224 To further confirm the direct regulation of PIC assembly by RPAP2, we utilized the
225 degradation tag (dTAG) system ([Nabet et al., 2018](#)) by integrating the Flag-FKBP12^{F36V} tag at
226 the N-terminus of the endogenous RPAP2 locus (RPAP2-dTAG) in DLD-1 cells (Figure 4E).
227 The addition of dTAG-13 for three hours induced a rapid depletion of RPAP2 protein in
228 RPAP2-dTAG cells (Figure 4F). Cellular fractionation showed a predominant presence of
229 RPAP2 in nucleoplasm and much less RPAP2 on chromatin (Figure 4G, row 1), in line with
230 our above results showing the mutually exclusive assembly of RPAP2-Pol II and PIC (Figure
231 3). Notably, rapid degradation of RPAP2 did not cause notably decreased association of Pol II
232 on chromatin or accumulation of Pol II in cytoplasm (Figure 4G, row 2), the observed effect
233 of siRNA-mediated RPAP2 silencing in previous study ([Forget et al., 2013](#)). This system
234 allowed us to evaluate the direct role of RPAP2 in PIC assembly without affecting RPAP2
235 function in transporting Pol II.

236 To determine whether and, if yes, to what extent the Pol II binding capacity and putative
237 phosphatase activity of RPAP2 contribute to its role in suppressing cellular PIC assembly, we
238 generated rescue cell lines by respectively inducing the expression of wildtype and mutant
239 RPAP2 in RPAP2-dTAG cells with rapid degradation of endogenous RPAP2 protein (Figure
240 4H, lanes 2-5). The two mutants include RPAP2^{A114-128}, which compromises Pol II interaction
241 (Figure 2E), and RPAP2^{Y127A}, which represents a phosphatase-dead mutant (Figure 2E) ([Irani
242 et al., 2016](#)). The comparison of TFIIF ChIP-Rx in dTAG-13 treated cells with induced
243 expression of wildtype RPAP2 and an empty pLVX-Tet-On vector showed higher levels of
244 TFIIF at promoters in the absence of RPAP2 (Figures 4I, 4K, and S5E, compare purple and
245 black), revealing the direct role of RPAP2 in prohibiting PIC assembly. Despite being
246 expressed to a higher level than wildtype RPAP2 (Figure 4H, lane 4), RPAP2^{A114-128} failed to
247 rescue the aberrant accumulation of TFIIF (Figure 4, J and K, compare green and black). In
248 contrast, the putative phosphatase-dead mutant RPAP2^{Y127A} fully restored the levels of TFIIF
249 as the wildtype RPAP2 did (Figure 4J, 4K, and S5E, compare skyblue and black). Heatmaps
250 showing the change of TFIIF levels indicated that wildtype RPAP2 and RPAP2^{Y127A}, but not
251 RPAP2^{A114-128}, regulate TFIIF occupancy at genome-wide levels (Figure 4L). These results
252 suggest that RPAP2 regulates a pre-initiation checkpoint through hindering the assembly of

253 PIC and thus the following transcription activation. Importantly, this function of RPAP2
254 requires its association with Pol II but not the reported phosphatase activity.

255 Discussion

256 Pol II-mediated transcription in metazoan is controlled at multiple levels including assembly
257 of PIC on core promoters, transcription initiation, Pol II CTD phosphorylation and promoter
258 escape, pausing and its release, elongation, and termination ([Chen et al., 2018](#); [Jonkers and Lis,](#)
259 [2015](#); [Taatjes, 2021](#)). Transcription checkpoints determine whether and when the transcription
260 machinery pauses or proceeds to ensure transcription is under precise control. One of the most
261 well-defined checkpoint is promoter-proximal Pol II pausing following the completion of
262 initiation ([Core and Adelman, 2019](#); [Smith and Shilatifard, 2013](#)) (Figure 4M, right panel). The
263 generation and maintenance of paused Pol II rely on the coordination of several pausing factors
264 including but not limited to the negative elongation factor (NELF), DRB sensitivity inducing
265 factor (DSIF) and Pol II-associated factor 1 (PAF1) ([Chen et al., 2018](#); [Core and Adelman,](#)
266 [2019](#)). Release of paused Pol II is driven by positive transcription elongation factor b (P-TEFb),
267 a cyclin-dependent kinase 9 (CDK9)-containing complex, which phosphorylates Pol II and
268 several key transcriptional regulators and thus activates the transcription machinery and
269 relieves negative factors such as NELF.

270 In this study, we demonstrated that RPAP2 serves as a pivotal transcription gatekeeper in
271 sterically inhibiting Pol II-TFIIF complex formation and transcription initiation. We proposed
272 a transcription checkpoint prior to PIC assembly, which we termed pre-initiation checkpoint
273 (Figure 4M, left panel). Given the critical role of TFIIF in stepwise PIC assembly ([Cortes et](#)
274 [al., 1992](#); [Flores et al., 1991](#)), an efficient transcription initiation requires the discharge of
275 RPAP2 from Pol II before the formation and loading of Pol II-TFIIF at promoters. Our in vitro
276 assays show that RPAP2 disrupts Pol II-TFIIF whereas TFIIF could not disrupt RPAP2-Pol II,
277 suggesting additional factor(s) or post-translational modifications is required to disrupt
278 RPAP2-Pol II and allow for Pol II-TFIIF formation.

279 The role of RPAP2/Rtr1 in transcription has mainly been attributed to its phosphatase activity
280 towards pSer5 of Pol II ([Ali et al., 2019](#); [Egloff et al., 2012](#); [Hsu et al., 2014](#); [Hunter et al.,](#)
281 [2016](#); [Irani et al., 2016](#); [Mosley et al., 2009](#); [Ni et al., 2014](#); [Victorino et al., 2020](#)). However,
282 this enzymatic activity is under debate due to the lack of a consensus phosphatase active pocket,
283 as evidenced by our structural study and others ([Irani et al., 2016](#); [Xiang et al., 2012](#)). Moreover,
284 despite being reported as an atypical phosphatase, RPAP2/Rtr1 possesses very low in vitro
285 phosphatase activity ([Hsu et al., 2014](#); [Irani et al., 2016](#)). Consistently, our in vitro assays
286 showed undetectable phosphatase activity of RPAP2 on phosphorylated Pol II CTD. Previous
287 studies suggested that RPRD1A-RPRD1B heterodimer facilitates RPAP2 phosphatase activity
288 by mediating RPAP2-Pol II association ([Ali et al., 2019](#); [Ni et al., 2014](#)). However, we found

289 that RPAP2 stably associates with Pol II (Pol IIa and Pol IIo) in the absence of RPRD1A-
290 RPRD1B and that RPRD1A-RPRD1B leads to no apparent impact on the conformation of
291 RPAP2-Pol II. In addition, our ChIP-Rx analyses showed that the phosphatase-dead mutant of
292 RPAP2 fully rescues the aberrant accumulation of TFIIF caused by RPAP2 loss, indicating
293 that RPAP2 modulates cellular PIC assembly independently of its putative phosphatase activity.
294 Regarding its function as a specific pSer5 phosphatase, we surmise that the induced
295 phosphorylation of Pol II upon RPAP2 depletion might partially result from effects of
296 enhanced PIC assembly and thus transcriptional activation. Supporting this notion, our results
297 showed that RPAP2 loss leads to a global increase in the occupancy of pSer2, which is not the
298 substrate of RPAP2 but will be induced by transcriptional activation.

299 The function of RPAP2 in disrupting Pol II-TFIIF interaction is reminiscent of Gdown1, which
300 also inhibits the binding of TFIIF to Pol II ([Cheng et al., 2012](#); [Jishage et al., 2012](#); [Wu et al.,](#)
301 [2012](#)), consistent with the critical role of TFIIF in Pol II-mediated transcription. However,
302 RPAP2 and Gdown1 regulate transcription in distinct stages. Gdown1 does not inhibit PIC
303 assembly or transcription initiation ([Mullen Davis et al., 2014](#)), but instead, negatively
304 regulates transcription at post-initiation stages ([Cheng et al., 2012](#); [DeLaney and Luse, 2016](#);
305 [Guo et al., 2014](#); [Jishage et al., 2012](#); [Jishage et al., 2018](#)). Reconciling these available lines of
306 evidence, we envision that activating signal-induced dissociation of RPAP2 and association of
307 TFIIF occurs before PIC assembly; Gdown1 then competes with TFIIF for Pol II binding to
308 hinder transcription at either pausing or elongation stages, given reported roles of TFIIF and
309 Gdown1 in both pausing and transcription elongation ([Cheng et al., 2012](#); [DeLaney and Luse,](#)
310 [2016](#); [Espinosa, 2012](#); [Joo et al., 2019](#); [Schweikhard et al., 2014](#)).

311 During the preparation of this manuscript, a structure of RPAP2-Pol II complex was reported
312 ([Fianu et al., 2021](#)), showing the incompatibility between RPAP2 and DNA in binding Pol II.
313 The structure is generally similar to our RPAP2-Pol II structure (Figure S3B). Intriguingly, gel
314 filtration analysis showed that the N-terminal region (1-215) of RPAP2 can be displaced from
315 Pol II during PIC assembly in a TATA box-binding protein (TBP)-based system ([Fianu et al.,](#)
316 [2021](#)). In contrast, we found that full-length RPAP2 is hardly displaced from Pol II and
317 prohibits Pol II-TFIIF interaction during PIC assembly in TFIID-based system. Consistently,
318 rapid degradation of RPAP2 leads to an aberrant accumulation of TFIIF at promoters with
319 unnoticeable defects in Pol II biogenesis and nuclear import. The above distinct observations
320 may result from differences in compositions of RPAP2 and PIC.

321 **References:**

- 322 Abdella, R., Talyzina, A., Chen, S., Inouye, C.J., Tjian, R., and He, Y. (2021). Structure of the human
323 Mediator-bound transcription preinitiation complex. *Science* 372, 52-56.
- 324 Adams, P.D., Afonine, P.V., Bunkoczi, G., Chen, V.B., Davis, I.W., Echols, N., Headd, J.J., Hung, L.W.,
325 Kapral, G.J., Grosse-Kunstleve, R.W., *et al.* (2010). PHENIX: a comprehensive Python-based system
326 for macromolecular structure solution. *Acta Crystallogr D Biol Crystallogr* 66, 213-221.
- 327 Ali, I., Ruiz, D.G., Ni, Z., Johnson, J.R., Zhang, H., Li, P.C., Khalid, M.M., Conrad, R.J., Guo, X., Min,
328 J., *et al.* (2019). Crosstalk between RNA Pol II C-Terminal Domain Acetylation and Phosphorylation
329 via RPRD Proteins. *Mol Cell* 74, 1164-1174 e1164.
- 330 Amemiya, H.M., Kundaje, A., and Boyle, A.P. (2019). The ENCODE Blacklist: Identification of
331 Problematic Regions of the Genome. *Sci Rep* 9, 9354.
- 332 Aoi, Y., Smith, E.R., Shah, A.P., Rendleman, E.J., Marshall, S.A., Woodfin, A.R., Chen, F.X.,
333 Shiekhattar, R., and Shilatifard, A. (2020). NELF Regulates a Promoter-Proximal Step Distinct from
334 RNA Pol II Pause-Release. *Mol Cell* 78, 261-274 e265.
- 335 Bernecky, C., Herzog, F., Baumeister, W., Plitzko, J.M., and Cramer, P. (2016). Structure of transcribing
336 mammalian RNA polymerase II. *Nature* 529, 551-554.
- 337 Buratowski, S., Hahn, S., Guarente, L., and Sharp, P.A. (1989). Five intermediate complexes in
338 transcription initiation by RNA polymerase II. *Cell* 56, 549-561.
- 339 Cevher, M.A., Shi, Y., Li, D., Chait, B.T., Malik, S., and Roeder, R.G. (2014). Reconstitution of active
340 human core Mediator complex reveals a critical role of the MED14 subunit. *Nat Struct Mol Biol* 21,
341 1028-1034.
- 342 Chen, F.X., Smith, E.R., and Shilatifard, A. (2018). Born to run: control of transcription elongation by
343 RNA polymerase II. *Nat Rev Mol Cell Biol* 19, 464-478.
- 344 Chen, V.B., Arendall, W.B., 3rd, Headd, J.J., Keedy, D.A., Immormino, R.M., Kapral, G.J., Murray,
345 L.W., Richardson, J.S., and Richardson, D.C. (2010). MolProbity: all-atom structure validation for
346 macromolecular crystallography. *Acta Crystallogr D Biol Crystallogr* 66, 12-21.
- 347 Chen, X., Qi, Y., Wu, Z., Wang, X., Li, J., Zhao, D., Hou, H., Li, Y., Yu, Z., Liu, W., *et al.* (2021a).
348 Structural insights into preinitiation complex assembly on core promoters. *Science* 372, eaba8490.
- 349 Chen, X., Yin, X., Li, J., Wu, Z., Qi, Y., Wang, X., Liu, W., and Xu, Y. (2021b). Structures of the human
350 Mediator and Mediator-bound preinitiation complex. *Science* 372, eabg0635.
- 351 Cheng, B., Li, T., Rahl, P.B., Adamson, T.E., Loudas, N.B., Guo, J., Varzavand, K., Cooper, J.J., Hu,
352 X., Gnatt, A., *et al.* (2012). Functional association of Gdown1 with RNA polymerase II poised on human
353 genes. *Mol Cell* 45, 38-50.
- 354 Core, L., and Adelman, K. (2019). Promoter-proximal pausing of RNA polymerase II: a nexus of gene
355 regulation. *Genes Dev* 33, 960-982.
- 356 Cortes, P., Flores, O., and Reinberg, D. (1992). Factors involved in specific transcription by mammalian
357 RNA polymerase II: purification and analysis of transcription factor IIA and identification of
358 transcription factor IIJ. *Mol Cell Biol* 12, 413-421.
- 359 DeLaney, E., and Luse, D.S. (2016). Gdown1 Associates Efficiently with RNA Polymerase II after
360 Promoter Clearance and Displaces TFIIF during Transcript Elongation. *PLoS One* 11, e0163649.
- 361 DeLano, W.L. (2002). The PyMOL Molecular Graphics System. on World Wide Web
362 <http://www.pymol.org>.

363 Egloff, S., Zaborowska, J., Laitem, C., Kiss, T., and Murphy, S. (2012). Ser7 phosphorylation of the
364 CTD recruits the RPAP2 Ser5 phosphatase to snRNA genes. *Mol Cell* *45*, 111-122.

365 Emsley, P., and Cowtan, K. (2004). Coot: model-building tools for molecular graphics. *Acta Crystallogr*
366 *D Biol Crystallogr* *60*, 2126-2132.

367 Espinosa, J.M. (2012). Get back TFIIIF, don't let me Gdown1. *Mol Cell* *45*, 3-5.

368 Feaver, W.J., Svejstrup, J.Q., Henry, N.L., and Kornberg, R.D. (1994). Relationship of CDK-activating
369 kinase and RNA polymerase II CTD kinase TFIIF/TFIIK. *Cell* *79*, 1103-1109.

370 Fianu, I., Dienemann, C., Aibara, S., Schilbach, S., and Cramer, P. (2021). Cryo-EM structure of
371 mammalian RNA polymerase II in complex with human RPAP2. *Commun Biol* *4*, 606.

372 Fisher, R.P., and Morgan, D.O. (1994). A novel cyclin associates with MO15/CDK7 to form the CDK-
373 activating kinase. *Cell* *78*, 713-724.

374 Flores, O., Lu, H., Killeen, M., Greenblatt, J., Burton, Z.F., and Reinberg, D. (1991). The small subunit
375 of transcription factor IIF recruits RNA polymerase II into the preinitiation complex. *Proc Natl Acad*
376 *Sci U S A* *88*, 9999-10003.

377 Forget, D., Lacombe, A.A., Cloutier, P., Lavalley-Adam, M., Blanchette, M., and Coulombe, B. (2013).
378 Nuclear import of RNA polymerase II is coupled with nucleocytoplasmic shuttling of the RNA
379 polymerase II-associated protein 2. *Nucleic Acids Res* *41*, 6881-6891.

380 Fujiwara, R., and Murakami, K. (2019). In vitro reconstitution of yeast RNA polymerase II transcription
381 initiation with high efficiency. *Methods* *159-160*, 82-89.

382 Gibney, P.A., Fries, T., Bailer, S.M., and Morano, K.A. (2008). Rtr1 is the *Saccharomyces cerevisiae*
383 homolog of a novel family of RNA polymerase II-binding proteins. *Eukaryot Cell* *7*, 938-948.

384 Goddard, T.D., Huang, C.C., Meng, E.C., Pettersen, E.F., Couch, G.S., Morris, J.H., and Ferrin, T.E.
385 (2018). UCSF ChimeraX: Meeting modern challenges in visualization and analysis. *Protein Sci* *27*, 14-
386 25.

387 Gotzke, H., Kilisch, M., Martinez-Carranza, M., Sograte-Idrissi, S., Rajavel, A., Schlichthaerle, T.,
388 Engels, N., Jungmann, R., Stenmark, P., Opazo, F., *et al.* (2019). The ALFA-tag is a highly versatile
389 tool for nanobody-based bioscience applications. *Nat Commun* *10*, 4403.

390 Guglielmi, V., Marini, M., Masson, E.F., Malatesta, M., Forget, D., Tomelleri, G., Coulombe, B., and
391 Vattemi, G. (2015). Abnormal expression of RNA polymerase II-associated proteins in muscle of
392 patients with myofibrillar myopathies. *Histopathology* *67*, 859-865.

393 Guo, J., Turek, M.E., and Price, D.H. (2014). Regulation of RNA polymerase II termination by
394 phosphorylation of Gdown1. *J Biol Chem* *289*, 12657-12665.

395 Guzder, S.N., Sung, P., Bailly, V., Prakash, L., and Prakash, S. (1994). RAD25 is a DNA helicase
396 required for DNA repair and RNA polymerase II transcription. *Nature* *369*, 578-581.

397 Hausmann, S., and Shuman, S. (2002). Characterization of the CTD phosphatase Fcp1 from fission
398 yeast. Preferential dephosphorylation of serine 2 versus serine 5. *J Biol Chem* *277*, 21213-21220.

399 Hsu, P.L., Yang, F., Smith-Kinnaman, W., Yang, W., Song, J.E., Mosley, A.L., and Varani, G. (2014).
400 Rtr1 is a dual specificity phosphatase that dephosphorylates Tyr1 and Ser5 on the RNA polymerase II
401 CTD. *J Mol Biol* *426*, 2970-2981.

402 Hunter, G.O., Fox, M.J., Smith-Kinnaman, W.R., Gogol, M., Fleharty, B., and Mosley, A.L. (2016).
403 Phosphatase Rtr1 Regulates Global Levels of Serine 5 RNA Polymerase II C-Terminal Domain
404 Phosphorylation and Cotranscriptional Histone Methylation. *Mol Cell Biol* *36*, 2236-2245.

405 Irani, S., Yogesha, S.D., Mayfield, J., Zhang, M., Zhang, Y., Matthews, W.L., Nie, G., Prescott, N.A.,
406 and Zhang, Y.J. (2016). Structure of *Saccharomyces cerevisiae* Rtr1 reveals an active site for an atypical
407 phosphatase. *Sci Signal* 9, ra24.

408 Jishage, M., Malik, S., Wagner, U., Uberheide, B., Ishihama, Y., Hu, X., Chait, B.T., Gnatt, A., Ren, B.,
409 and Roeder, R.G. (2012). Transcriptional regulation by Pol II(G) involving mediator and competitive
410 interactions of Gdown1 and TFIIF with Pol II. *Mol Cell* 45, 51-63.

411 Jishage, M., Yu, X., Shi, Y., Ganesan, S.J., Chen, W.Y., Sali, A., Chait, B.T., Asturias, F.J., and Roeder,
412 R.G. (2018). Architecture of Pol II(G) and molecular mechanism of transcription regulation by Gdown1.
413 *Nat Struct Mol Biol* 25, 859-867.

414 Jonkers, I., and Lis, J.T. (2015). Getting up to speed with transcription elongation by RNA polymerase
415 II. *Nat Rev Mol Cell Biol* 16, 167-177.

416 Joo, Y.J., Ficarro, S.B., Chun, Y., Marto, J.A., and Buratowski, S. (2019). In vitro analysis of RNA
417 polymerase II elongation complex dynamics. *Genes Dev* 33, 578-589.

418 Kastner, B., Fischer, N., Golas, M.M., Sander, B., Dube, P., Boehringer, D., Hartmuth, K., Deckert, J.,
419 Hauer, F., Wolf, E., *et al.* (2008). GraFix: sample preparation for single-particle electron
420 cryomicroscopy. *Nat Methods* 5, 53-55.

421 Kim, M., Suh, H., Cho, E.J., and Buratowski, S. (2009). Phosphorylation of the yeast Rpb1 C-terminal
422 domain at serines 2, 5, and 7. *J Biol Chem* 284, 26421-26426.

423 Li, H., Handsaker, B., Wysoker, A., Fennell, T., Ruan, J., Homer, N., Marth, G., Abecasis, G., Durbin,
424 R., and Genome Project Data Processing, S. (2009). The Sequence Alignment/Map format and
425 SAMtools. *Bioinformatics* 25, 2078-2079.

426 Lin, Y.C., Choi, W.S., and Gralla, J.D. (2005). TFIIF XPB mutants suggest a unified bacterial-like
427 mechanism for promoter opening but not escape. *Nat Struct Mol Biol* 12, 603-607.

428 Mastronarde, D.N. (2005). Automated electron microscope tomography using robust prediction of
429 specimen movements. *J Struct Biol* 152, 36-51.

430 Mosley, A.L., Pattenden, S.G., Carey, M., Venkatesh, S., Gilmore, J.M., Florens, L., Workman, J.L.,
431 and Washburn, M.P. (2009). Rtr1 is a CTD phosphatase that regulates RNA polymerase II during the
432 transition from serine 5 to serine 2 phosphorylation. *Mol Cell* 34, 168-178.

433 Mullen Davis, M.A., Guo, J., Price, D.H., and Luse, D.S. (2014). Functional interactions of the RNA
434 polymerase II-interacting proteins Gdown1 and TFIIF. *J Biol Chem* 289, 11143-11152.

435 Nabet, B., Roberts, J.M., Buckley, D.L., Paulk, J., Dastjerdi, S., Yang, A., Leggett, A.L., Erb, M.A.,
436 Lawlor, M.A., Souza, A., *et al.* (2018). The dTAG system for immediate and target-specific protein
437 degradation. *Nat Chem Biol* 14, 431-441.

438 Ni, Z., Xu, C., Guo, X., Hunter, G.O., Kuznetsova, O.V., Tempel, W., Marcon, E., Zhong, G., Guo, H.,
439 Kuo, W.W., *et al.* (2014). RPRD1A and RPRD1B are human RNA polymerase II C-terminal domain
440 scaffolds for Ser5 dephosphorylation. *Nat Struct Mol Biol* 21, 686-695.

441 Orlando, D.A., Chen, M.W., Brown, V.E., Solanki, S., Choi, Y.J., Olson, E.R., Fritz, C.C., Bradner, J.E.,
442 and Guenther, M.G. (2014). Quantitative ChIP-Seq normalization reveals global modulation of the
443 epigenome. *Cell Rep* 9, 1163-1170.

444 Pettersen, E.F., Goddard, T.D., Huang, C.C., Couch, G.S., Greenblatt, D.M., Meng, E.C., and Ferrin,
445 T.E. (2004). UCSF Chimera--a visualization system for exploratory research and analysis. *Journal of*
446 *computational chemistry* 25, 1605-1612.

- 447 Ramirez, F., Ryan, D.P., Gruning, B., Bhardwaj, V., Kilpert, F., Richter, A.S., Heyne, S., Dundar, F., and
448 Manke, T. (2016). deepTools2: a next generation web server for deep-sequencing data analysis. *Nucleic*
449 *Acids Res* *44*, W160-165.
- 450 Rengachari, S., Schilbach, S., Aibara, S., Dienemann, C., and Cramer, P. (2021). Structure of the human
451 Mediator-RNA polymerase II pre-initiation complex. *Nature*.
- 452 Roeder, R.G. (1996). The role of general initiation factors in transcription by RNA polymerase II.
453 *Trends Biochem Sci* *21*, 327-335.
- 454 Schweikhard, V., Meng, C., Murakami, K., Kaplan, C.D., Kornberg, R.D., and Block, S.M. (2014).
455 Transcription factors TFIIF and TFIIS promote transcript elongation by RNA polymerase II by
456 synergistic and independent mechanisms. *Proc Natl Acad Sci U S A* *111*, 6642-6647.
- 457 Smith, E., and Shilatifard, A. (2013). Transcriptional elongation checkpoint control in development and
458 disease. *Genes Dev* *27*, 1079-1088.
- 459 Smith-Kinnaman, W.R., Berna, M.J., Hunter, G.O., True, J.D., Hsu, P., Cabello, G.I., Fox, M.J., Varani,
460 G., and Mosley, A.L. (2014). The interactome of the atypical phosphatase Rtr1 in *Saccharomyces*
461 *cerevisiae*. *Mol Biosyst* *10*, 1730-1741.
- 462 Taatjes, D.J. (2021). RNA Polymerase II Transcription. *J Mol Biol* *433*, 167037.
- 463 Thomas, M.C., and Chiang, C.M. (2006). The general transcription machinery and general cofactors.
464 *Crit Rev Biochem Mol Biol* *41*, 105-178.
- 465 Victorino, J.F., Fox, M.J., Smith-Kinnaman, W.R., Peck Justice, S.A., Burriss, K.H., Boyd, A.K.,
466 Zimmerly, M.A., Chan, R.R., Hunter, G.O., Liu, Y., *et al.* (2020). RNA Polymerase II CTD phosphatase
467 Rtr1 fine-tunes transcription termination. *PLoS Genet* *16*, e1008317.
- 468 Vos, S.M., Farnung, L., Urlaub, H., and Cramer, P. (2018). Structure of paused transcription complex
469 Pol II-DSIF-NELF. *Nature* *560*, 601-606.
- 470 Wu, Y.M., Chang, J.W., Wang, C.H., Lin, Y.C., Wu, P.L., Huang, S.H., Chang, C.C., Hu, X., Gnatt, A.,
471 and Chang, W.H. (2012). Regulation of mammalian transcription by Gdown1 through a novel steric
472 crosstalk revealed by cryo-EM. *EMBO J* *31*, 3575-3587.
- 473 Xiang, K., Manley, J.L., and Tong, L. (2012). The yeast regulator of transcription protein Rtr1 lacks an
474 active site and phosphatase activity. *Nat Commun* *3*, 946.
- 475 Zowel, L., and Reinberg, D. (1993). Initiation of transcription by RNA polymerase II: a multi-step
476 process. *Prog Nucleic Acid Res Mol Biol* *44*, 67-108.
- 477 Zhang, K. (2016). Gctf: Real-time CTF determination and correction. *J Struct Biol* *193*, 1-12.
- 478 Zhang, Y., Kim, Y., Genoud, N., Gao, J., Kelly, J.W., Pfaff, S.L., Gill, G.N., Dixon, J.E., and Noel, J.P.
479 (2006). Determinants for dephosphorylation of the RNA polymerase II C-terminal domain by Scp1.
480 *Mol Cell* *24*, 759-770.
- 481 Zhang, Y., Zhang, M., and Zhang, Y. (2011). Crystal structure of Ssu72, an essential eukaryotic
482 phosphatase specific for the C-terminal domain of RNA polymerase II, in complex with a transition
483 state analogue. *Biochem J* *434*, 435-444.
- 484 Zheng, H., Qi, Y., Hu, S., Cao, X., Xu, C., Yin, Z., Chen, X., Li, Y., Liu, W., Li, J., *et al.* (2020).
485 Identification of Integrator-PP2A complex (INTAC), an RNA polymerase II phosphatase. *Science* *370*,
486 eabb5872.
- 487 Zheng, S.Q., Palovcak, E., Armache, J.P., Verba, K.A., Cheng, Y., and Agard, D.A. (2017). MotionCor2:
488 anisotropic correction of beam-induced motion for improved cryo-electron microscopy. *Nature methods*

489 *14*, 331-332.
490 Zivanov, J., Nakane, T., Forsberg, B.O., Kimanius, D., Hagen, W.J., Lindahl, E., and Scheres, S.H.
491 (2018). New tools for automated high-resolution cryo-EM structure determination in RELION-3. *Elife*
492 *7*.
493

494 **Acknowledgments:** We thank the Center of Cryo-Electron Microscopy of Fudan University
495 for the supports on data collection and the Biomedical Core Facility, Fudan University for the
496 support on mass spectrometry analyses. This work was supported by grants from the National
497 key R&D program of China (2016YFA0500700), the National Natural Science Foundation of
498 China (32030055, 31830107, 31821002), the Shanghai Municipal Science and Technology
499 Major Project (2017SHZDZX01), Shanghai Municipal Science and Technology Commission
500 (19JC1411500), the National Ten-Thousand Talent Program (Y. X.), the National Program for
501 support of Top-Notch Young Professionals (Y. X.), and the Strategic Priority Research
502 Program of the Chinese Academy of Sciences (grant no. XDB08000000).

503

504 **Author contributions:** C. X. and X. W. prepared the samples for structural and biochemical
505 analyses with the help from J. L., D. Z. and H. Z.; Y. Q. performed the cryo-EM analyses and
506 the model building; Z. W. and L. W. generated the knock-in cell lines and conducted
507 sequencing experiments with the help from Q.J.; A. S. analyzed the sequencing data; Y. X.,
508 F.X.C., and X. C. wrote the manuscript; Y. X. supervised the project.

509

510 **Competing interests:** Authors declare no competing interests.

511 **Data and materials availability:** The cryo-EM maps have been deposited in the Electron
512 Microscopy Data Bank (EMDB) with accession numbers of 31450 and 31451 and the structure
513 coordinate has been deposited in the Protein Data Bank (PDB) with the accession number of
514 7F4G.

515 **Materials and Methods**

516 **Antibodies and cell culture**

517 Antibodies were as follows: Pol II (NTD) (#14958, Cell Signaling), Pol II (pSer2)
518 (#13499, Cell Signaling), GTF2F1 (10093-2-AP, Proteintech), FLAG (#SLAB01, Smart
519 Lifesciences), histone H3 (#4499, Cell Signaling), TBP: (66166-1-Ig, Proteintech). RPAP2
520 antibody is generated by Abclonal. 293T, DLD-1 and MEF cells were grown in DMEM
521 supplemented with 10% FBS.

522 **Protein expression and purification**

523 The 12 full-length open reading frames (ORFs) of human Pol II subunits were amplified
524 from 293T cDNA by PCR or synthesized and sub-cloned into a modified pCAG vector and
525 RPB1 was tagged with a C-terminal Protein A. All plasmids were co-transfected to Expi293F
526 cells using PEI. After cultured at 37°C for 48 h, cells were harvested and lysed in buffer
527 containing 30 mM HEPES pH 8.0, 300 mM NaCl, 0.25% CHAPS, 5 mM ATP, 5 mM MgCl₂,
528 1 mM EDTA, 10 μM ZnCl₂, 3 mM DTT, 10% Glycerol (v/v), 1 mM PMSF, 1 μg/mL Aprotinin,
529 1 μg/mL Pepstatin, 1 μg/mL Leupeptin at 4°C for 30 min. The cell lysate was clarified by
530 centrifugation at 15,000 rpm at 4°C for 30 min and the supernatant was incubated with IgG
531 resin (Smart-Lifesciences) for 1.5 h followed by on-column digestion at 4°C overnight in buffer
532 containing 30 mM HEPES pH 8.0, 300 mM NaCl, 0.1% CHAPS, 1 mM EDTA, 2 mM MgCl₂,
533 10 μM ZnCl₂, 3 mM DTT, 10% Glycerol (v/v). The immobilized proteins were eluted out and
534 further purified by a mono Q 5/5 column (GE Healthcare) and a Superose S6 Increase 5/150
535 GL column (GE Healthcare) in buffer containing 30 mM HEPES pH 8.0, 150 mM NaCl, 2 mM
536 MgCl₂, 0.2 mM EDTA, 10 μM ZnCl₂ and 1mM TCEP. The peak fractions corresponding to
537 the RPAP2-Pol II complex were concentrated using a 100-kDa cut-off centrifugation filter unit
538 (Amicon Ultra). The purified complex was used for cryo-EM.

539 Human RPAP2 was sub-cloned into a modified pCAG containing an N-terminal protein
540 A tag. The plasmid was transfected to Expi293F cells using PEI. After cultured at 37°C for 72
541 h, cells were harvested and lysed in Lysis buffer containing 30 mM HEPES pH 8.0, 300 mM
542 NaCl, 0.25% CHAPS, 5 mM ATP, 5 mM MgCl₂, 1mM EDTA, 10 μM ZnCl₂, 3 mM DTT, 10%
543 Glycerol (v/v), 1 mM PMSF, 1 μg/mL Aprotinin, 1 μg/mL Pepstatin, 1 μg/mL Leupeptin at
544 4°C for 30 min. Clarified lysates were applied to IgG resin (Smart-Lifesciences) for 1.5 h
545 followed by on-column digestion at 4°C for 1 h. The immobilized proteins were eluted and
546 further purified by a mono Q 5/5 column (GE Healthcare) and a Superdex75 10/300 GL column
547 (GE Healthcare) in a buffer containing 30 mM HEPES pH 7.9, 100 mM KCl, 10 μM ZnCl₂, 1

548 mM TCEP, 5% Glycerol (v/v). The peak fractions were pooled, aliquoted, snap frozen and
549 stored at -80°C.

550 RPRD1A-RPRD1B complex was prepared essentially in a similar scheme. The two full-
551 length ORFs of human RPRD1A and RPRD1B were separately sub-cloned into a modified
552 pCAG vector containing N-terminal Protein A (ProA) tag and co-expressed in Expi293F cells.
553 After cell lysis, the lysate was applied onto the IgG (Smart-Lifesciences) affinity
554 chromatography column, followed by on-column digestion and the eluate was further purified
555 by a mono Q 5/5 column (GE Healthcare) and a Superdex75 10/300 GL column (GE
556 Healthcare) in buffer containing 30 mM HEPES pH 7.9, 100 mM KCl, 1 mM TCEP, 5%
557 Glycerol (v/v). The peak fractions containing RPRD1A-RPRD1B complex were pooled,
558 aliquoted, snap frozen and stored at -80°C.

559 GTFs (TFIID, TFIIA, TFIIB, TFIIF, TFIIE, TFIIH), *HDM2* promoter DNA, TFIID-
560 TFIIA-promoter were prepared as previously described ([Chen et al., 2021a](#)). Unphosphorylated
561 Pol II was isolated from *S. scrofa* thymus and purified following previously established
562 protocol ([Vos et al., 2018](#)). Four residue substitutions (G882S of RBP2, T75I of RPB3, S140N
563 of RPB3, and S126T of RPB6) exist between *S. scrofa* and *H. sapiens* Pol II. The
564 phosphorylated Pol II was prepared by in vitro phosphorylation using TFIIH as previously
565 described ([Zheng et al., 2020](#)).

566

567 **In vitro pull-down assay**

568 In the RPAP2 pulldown assay, the purified RPAP2 was incubated with phosphorylated
569 Pol II or unphosphorylated Pol II at 4°C for 2h in 400 µl Binding buffer containing 30 mM
570 HEPES-KOH pH 7.9, 100 mM KCl, 0.05% CHAPS, 2mM MgCl₂, 2 mM DTT, 0.2 mM EDTA,
571 10 µM ZnCl₂ and 5% (v/v) glycerol. RPAP2 antibody (αRPAP2) and protein G resins were
572 incubated at 4°C for 2h. Subsequently, the resins were washed three times and added to the
573 RPAP2 and phosphorylated Pol II/ unphosphorylated Pol II mixture for another 2 hours at 4°
574 C. The resins were extensively washed with the Binding buffer, and the bound proteins were
575 subjected to SDS-PAGE followed by Coomassie blue staining.

576 In the 8WG16 pulldown assay, the purified RPAP2 mutants/truncations were individually
577 incubated with purified Pol II at 4°C for 2h in Binding buffer, followed by the addition of Pol
578 II antibody (8WG16) and protein G resins and further incubation at 4°C for 2h. After
579 extensively washed using Binding buffer, the bound proteins were subjected to SDS-PAGE
580 followed by Coomassie blue staining.

581 In the IgG pulldown assay, the indicated plasmids of N-terminal Protein A tagged RPAP2
582 mutants and truncations were individually transfected to Expi293F cells and cultured at 37°C
583 for 72h. Cells of each RPAP2 protein were separately lysed as described above. The
584 supernatant of cell lysate was incubated with IgG resins at 4°C for 2h. The resins were washed
585 three times and resuspended 400 µl Binding buffer. The purified unphosphorylated Pol II was
586 then added and incubated with the resins at 4°C for 2h. The resins were extensively washed
587 and the bound proteins were subjected to SDS-PAGE and stained by Coomassie blue.

588

589 **In vitro phosphatase assay**

590 In vitro phosphatase assay was performed as previously described ([Zheng et al., 2020](#)).
591 Briefly, the phosphorylated Pol II (0.1 µM) was incubated with RPAP2 (2 µM, 10 µM) or
592 INTAC complex (0.4 µM) in a final volume of 20 µl containing 50 mM HEPES-NaOH pH 7.4,
593 100 mM NaCl, 0.01% CHAPS, 10mM MgCl₂, 1mM MnCl₂, and 2 mM DTT. The reactions
594 were performed at 30°C for 30 min and stopped by adding 5 µl of 5 × SDS loading buffer.
595 Samples (2.5 µl) were subjected to SDS-PAGE and analyzed by Western blotting with
596 indicated antibodies.

597

598 **In vitro competitive binding Assay**

599 The competitive binding assay for RPAP2 and Pol II-TFIIF. The plasmids of N-terminal
600 ALFA-tagged ([Gotzke et al., 2019](#)) TFIIF (ALFA-tagged TFIIF α and untagged TFIIF β) were
601 co-transfected to Expi293F cells and cultured at 37°C for 72h. Cells were pelleted and lysed as
602 described above. The supernatant of cell lysate was incubated with ALFA-nanobody
603 (α ALFA) coupled resin at 4°C for 2h. The resins were washed three times and resuspended in
604 Binding buffer. Subsequently, the purified unphosphorylated Pol II was added and incubated
605 with the resins at 4°C for 2h. The resins were washed three times to remove unbound Pol II,
606 followed by the addition of an equal amount of RPAP2 and further incubated for 2 hours. The
607 resins were extensively washed and subjected to SDS-PAGE and stained by Coomassie blue.

608 The competitive binding assay for PIC components (TFIID-TFIIA-promoter, TFIIB,
609 TFIIF, TFIIE and TFIIH) and RPAP2-Pol II. The purified RPAP2 was incubated with
610 unphosphorylated Pol II at 4°C for 2h in 400 µl Binding buffer. RPAP2 antibody (α RPAP2)
611 and protein G resins were incubated at 4°C for 2h. Subsequently, the resins were washed three
612 times and added to pre-assembled RPAP2-Pol II for another 2 hours at 4°C. The resins were

613 washed three times to remove unbound Pol II, followed by the addition of three molar excess
614 of TFIID-TFIIA-promoter, TFIIB, TFIIF, TFIIE or TFIIH and further incubated for 2 hours.
615 10 μ M THZ1 (MedChemExpress) was added to the reaction containing TFIIH to impaired the
616 kinase activity of TFIIH. The resins were extensively washed with the Binding buffer, and the
617 bound proteins were subjected to SDS-PAGE followed by Coomassie blue staining.

618

619 **Glycerol density gradient ultracentrifugation and competitive assay**

620 To assemble the RPAP2-Pol II complex, 60 pmol of the purified *S. scrofa*
621 unphosphorylated Pol II was incubated with 2-fold molar excess of purified RPAP2 at 4°C for
622 3h, and then added on top of a 4 ml 10%-50% (w/v) glycerol gradient in buffer containing 30
623 mM HEPES-KOH pH 7.9, 100 mM KCl, 2 mM MgCl₂, 2 mM DTT and centrifuged for 16 h
624 at 34,000 rpm at 4°C for 16 h using an SW60 Ti rotor (Beckman Coulter). The fractions, 200 μ l
625 each, were subjected to SDS-PAGE and Coomassie blue staining. The peak fractions
626 containing Pol II-RPAP2 complex were pooled, concentrated, aliquoted, snap frozen and stored
627 at -80°C. The assembly of Pol II-TFIIF complex was prepared and analysis in a similar scheme.

628 To test the binding of RPAP2 and Pol II in the presence of excess TFIIF, 60 pmol of the
629 purified *S. scrofa* unphosphorylated Pol II was pre-incubated with 2-fold molar excess of
630 purified RPAP2 at 4°C for 1 h, followed by the addition of 5-fold molar excess of TFIIF and
631 further incubation at 4°C for 2 h. The sample was subjected to glycerol density gradient
632 ultracentrifugation as above mentioned.

633 The test of the binding of TFIIF and Pol II in the presence of excess RPAP2 were
634 performed in a similar way. 5-fold molar excess of RPAP2 was incubated with 60 pmol of pre-
635 incubated Pol II-TFIIF, and then analysis by glycerol density gradient ultracentrifugation.

636 To test the assembly of RPAP2-Pol II-RPRD1A-RPRD1B complex, The purified *S.*
637 *scrofa* Pol II was incubated with RPAP2 and RPRD1A-PRD1B in molar ratio of 1:2:5 at 4°C
638 for 3h, followed by glycerol density gradient ultracentrifugation in buffer containing 10%-50%
639 (w/v) glycerol, 30 mM HEPES-KOH pH 7.9, 100 mM NaCl, 2 mM MgCl₂, 10 μ M ZnCl₂, 2
640 mM DTT and centrifuged for 16 h at 34,000 rpm at 4°C for 16 h using an SW60 Ti rotor
641 (Beckman Coulter). The fractions were subjected to SDS-PAGE and Coomassie blue staining.

642

643 **Cryo-EM sample preparation**

644 To assemble the RPAP2-Pol II-RPRD1A-RPRD1B complex for cryo-EM sample
645 preparation. The purified *S. scrofa* Pol II was incubated with RPAP2 and RPRD1A-PRD1B in

646 molar ratio of 1:2:5 at 4°C for 3h. The mixture was then subjected to GraFix ([Kastner et al.,](#)
647 [2008](#)). The glycerol gradient was prepared using light buffer containing 10% (w/v) glycerol,
648 30 mM HEPES-KOH pH 7.9, 100 mM NaCl, 2 mM MgCl₂, 10 μM ZnCl₂, 2 mM DTT, and
649 heavy buffer containing 50% (w/v) glycerol, 30 mM HEPES-KOH pH 7.9, 100 mM NaCl, 2
650 mM MgCl₂, 10 μM ZnCl₂, 2 mM DTT, and 0.005% glutaraldehyde. The samples were
651 centrifuged at 34,000 rpm at 4°C for 16 h using an SW60 Ti rotor (Beckman Coulter).
652 Subsequently, fractions containing cross-linked complexes were quenched with 50 mM Tris
653 pH 7.4 (25°C). The homogeneity of peak fractions was assessed by negative stain EM.
654 Fractions of interest were pooled, concentrated, followed by buffer exchange into a buffer
655 containing 30 mM HEPES-KOH pH 7.9, 100 mM NaCl, 2 mM MgCl₂, 10 μM ZnCl₂, 2mM
656 DTT, and 0.8 % (v/v) glycerol.

657 For negative-stain EM, 5 μl of freshly purified protein sample was applied onto a glow-
658 discharged copper grid supported by a continuous thin layer of carbon film for 60 s before
659 negative staining by 2% (w/v) uranyl formate at room temperature. The negatively stained grid
660 was loaded onto a FEI Talos L120C microscope operated at 120 kV, equipped with a Ceta
661 CCD camera.

662 For cryo-EM grid preparation, 4 μl of protein sample (about 1.5 mg/ml) was applied onto
663 a glow-discharged holey carbon grid (Quantifoil Au, R1.2/1.3, 300 mesh). At a temperature of
664 4°C and under a humidity of 100%, the grid was blotted for 6 s using a FEI Vitrobot Mark IV
665 and plunge frozen in liquid ethane cooled by liquid nitrogen. The grids were prepared in the
666 H₂/O₂ mixture for 20 s using a Gatan 950 Solarus plasma cleaning system with a power of 5
667 W.

668

669 **Data collection**

670 The cryo-EM grids of human RPAP2-Pol II and RPAP2-Pol II -RPRD1A-RPRD1B were
671 loaded onto a Thermo Fisher Scientific Titan Krios transmission electron microscope equipped
672 with a Gatan K2 direct electron detector and operating at 300kV for data collection. For
673 RPAP2-Pol II, all the cryo-EM images were automatically recorded in the super-resolution
674 counting mode using Serial-EM ([Mastrorade, 2005](#)) with a nominal magnification of
675 105,000x, which yielded a super-resolution pixel size of 0.678 Å, and with a defocus ranged
676 from 1.8 to 2.5 μm. For RPAP2-Pol II-RPRD1A-RPRD1B, all the cryo-EM images were
677 automatically recorded in the super-resolution counting mode using Serial-EM with a nominal
678 magnification of 130,000x, which yielded a super-resolution pixel size of 0.522 Å, and with a

679 defocus ranged from 1.8 to 2.5 μm . Each micrograph stack was dose-fractionated to 32 frames
680 with a total electron dose of $\sim 50 \text{ e}^-/\text{\AA}^2$. 1,505 micrographs of RPAP2-Pol II and 2,529
681 micrographs of RPAP2-Pol II -RPRD1A-RPRD1B were collected for further processing.

682

683 **Image processing**

684 For cryo-EM data, drift and beam-induced motion correction were applied on the super
685 resolution movie stacks using MotionCor2([Zheng et al., 2017](#)) and binned twofold to a
686 calibrated pixel size of 1.356 $\text{\AA}/\text{pixel}$ and 1.044 $\text{\AA}/\text{pixel}$, respectively. The defocus values were
687 estimated by Gctf ([Zhang, 2016](#)) from summed images without dose weighting. Other
688 procedures of cryo-EM data processing were performed using RELION 3.0([Zivanov et al.,](#)
689 [2018](#)) and cryoSPARC using dose-weighted micrographs.

690 For human RPAP2-Pol II, a subset of $\sim 10,000$ particles were picked by RELION 3.0
691 without reference and subjected to reference-free 2D classification. Some of the resulting 2D
692 class averages were low-pass filtered to 20 \AA and used as references for automatic particle
693 picking of the whole datasets in RELION resulting in an initial set of 1,593,921 particles for
694 reference-free 2D classification. 862,194 particles were selected after several rounds 3D
695 classifications, using a 60 \AA low-pass filtered initial model from our previous cryo-EM
696 reconstruction. 543,699 particles in four of the selected eight classes were imported to a 3D
697 auto-refine and Postprocess, yielding a reconstruction of the RPAP2-Pol II complex at 3.5 \AA
698 resolution. For the RPAP2 module, two rounds of local mask 3D classification were performed.
699 85,919 particles in one of the selected three classes were imported to a 3D auto-refine and
700 Postprocess, yielding a 4.5 \AA reconstruction.

701 For RPAP2-Pol II-RPRD1A-RPRD1B, a subset of $\sim 10,000$ particles were picked by
702 RELION 3.0 without reference and subjected to reference-free 2D classification. Some of the
703 resulting 2D class averages were low-pass filtered to 20 \AA and used as references for automatic
704 particle picking of the whole datasets in RELION resulting in an initial set of 1,173,686
705 particles for reference-free 2D classification. 754,747 particles were selected after several
706 rounds of 3D classifications, using a 60 \AA low-pass filtered initial model from our previous
707 cryo-EM reconstruction. 646,517 particles in one of the selected six classes were imported to
708 a cryoSPARC package for NU-refinement and sharpening, yielding a reconstruction of the
709 RPAP2-Pol II-RPRD1-RPRD1B at 2.8 \AA resolution. For the RPAP2 module, a local mask 3D
710 classification were performed. 164,816 particles in one of the selected eight classes were
711 imported to a cryoSPARC package for local refinement and sharpening, yielding a 3.4 \AA
712 reconstruction.

713 All reported resolutions were calculated based on the gold-standard Fourier shell
714 correlation (FSC)=0.143 criterion. The GSFSC curves were corrected for the effects of a soft
715 mask with high-resolution noise substitution. All cryo-EM maps were sharpened by applying
716 a negative B-factor estimated in RELION. All the visualization and evaluation of the 3D
717 volume map were performed within UCSF Chimera ([Pettersen et al., 2004](#)) or UCSF ChimeraX
718 ([Goddard et al., 2018](#)), and the local resolution variations were calculated using RELION.

719

720 **Model building and structure refinement**

721 The cryo-EM maps of RPAP2-Pol II-RPRD1A-RPRD1B (2.8 Å) and locally refined maps
722 of RPAP2 (3.4 Å) were used for model building.

723 The following structural templates were used as references for model building. The
724 structural templates include the cryo-EM structure of Pol II (PDB: 7EGB) ([Chen et al., 2021a](#))
725 and yeast Rtr1 (PDB: 4FC8) ([Xiang et al., 2012](#)). These structural models were docked into
726 corresponding cryo-EM maps, followed by rigid-body fitting using UCSF Chimera([Pettersen
727 et al., 2004](#)) and manual adjustment in COOT([Emsley and Cowtan, 2004](#)). Atomic structural
728 models of Pol II and RPAP2 were built according to cryo-EM maps and refined in real space
729 using Phenix([Adams et al., 2010](#)).

730 Statistics of the map reconstruction and model refinement are shown in Table S1. The
731 final models were evaluated using MolProbity ([Chen et al., 2010](#)). Model representations in
732 the figures and movies were prepared by PyMOL ([DeLano, 2002](#)) or UCSF ChimeraX
733 ([Goddard et al., 2018](#)).

734

735 **In vitro transcription initiation assay**

736 GTFs and *HDM2* promotor DNA were prepared as previously described ([Chen et al.,
737 2021a](#)). In vitro transcription initiation assay was performed as previously described ([Cevher
738 et al., 2014](#); [Fujiwara and Murakami, 2019](#)). Briefly, 1.3 pmol of *HDM2* promoter DNA was
739 combined with 1.5 pmol of TFIID, 3 pmol of TFIIA, 3 pmol of TFIIB, 3 pmol of TFIIF, 3 pmol
740 of TFIIE, 1.5 pmol of TFIIH, either 2 pmol of *S. scrofa* Pol II with increasing amount of
741 RPAP2 (0 pmol, 2 pmol, 4 pmol, 8 pmol) or 2 pmol RPAP2-Pol II complex in a volume of 10
742 µl containing 30 mM HEPES pH 7.9, 100 mM KCl, 6 mM MgCl₂, 2 mM DTT, 5% (v/v)
743 glycerol for 30 min at 25°C. Reactions were initiated by the addition an equal volume of buffer
744 containing 24 mM HEPES-KOH pH 8.0, 120 mM KCl, 10 mM MgCl₂, 1.2 mM DTT, 24%
745 (v/v) glycerol, 100 µg/ml BSA, 200 µM GTP, 200 µM CTP, 200 µM ATP, 200 µM UTP, and

746 99 nM [α -³²P] UTP. The reactions were incubated at 25°C for 30 min and then were subjected
747 to urea polyacrylamide gels and autoradiography.

748

749 **Generating dTAG endogenous knock-in and rescues cell lines**

750 To generate RPAP2-dTAG cells by the endogenous knock-in, PITCh sgRNA/Cas9 and
751 donor plasmids were mixed with 1×10^6 DLD-1 cells followed by electroporation. After
752 recovering for 2 days without antibiotic selection, cells were serially diluted and cultured with
753 1 μ g/ml puromycin for 10-14 days. Single-clone colonies were picked, expanded, and
754 genotyped by genomic DNA PCR targeting the integration site. For homogeneous knock-in
755 clones, protein degradation efficiency was verified by DMSO and dTAG-13 treatment for 3
756 hours followed by western blotting.

757 To generate rescue cell lines, RPAP2-dTAG cells were initially infected with lentivirus
758 expressing pLVX-Tet3G and cultured with neomycin for 2 weeks. Stable cells were transduced
759 with lentivirus expressing wildtype RPAP2, RPAP2 Δ ¹¹⁴⁻¹²⁸, or RPAP2^{Y127A} cloned into pLVX-
760 Tet-On vector with Blasticidin resistance gene, and then selected with antibiotics for 2 weeks.

761 **RNA interference**

762 Lentivirus expressing short-hairpin RNAs was prepared by transfecting PLKO.1 shRNA
763 plasmids and packaging plasmids containing psPAX2 and pMD2.G into 293T cells using PEI
764 (Polysciences). Collected conditional media containing virus particles were used to transduce
765 cells in the growth media supplemented with Polybrene for 24 hours. The infected cells were
766 selected with 2 μ g/ml puromycin for an extra 48 hours. The cells were then switched into
767 growth media without antibiotics and grown for an additional 24 hours before being harvested
768 for further analysis.

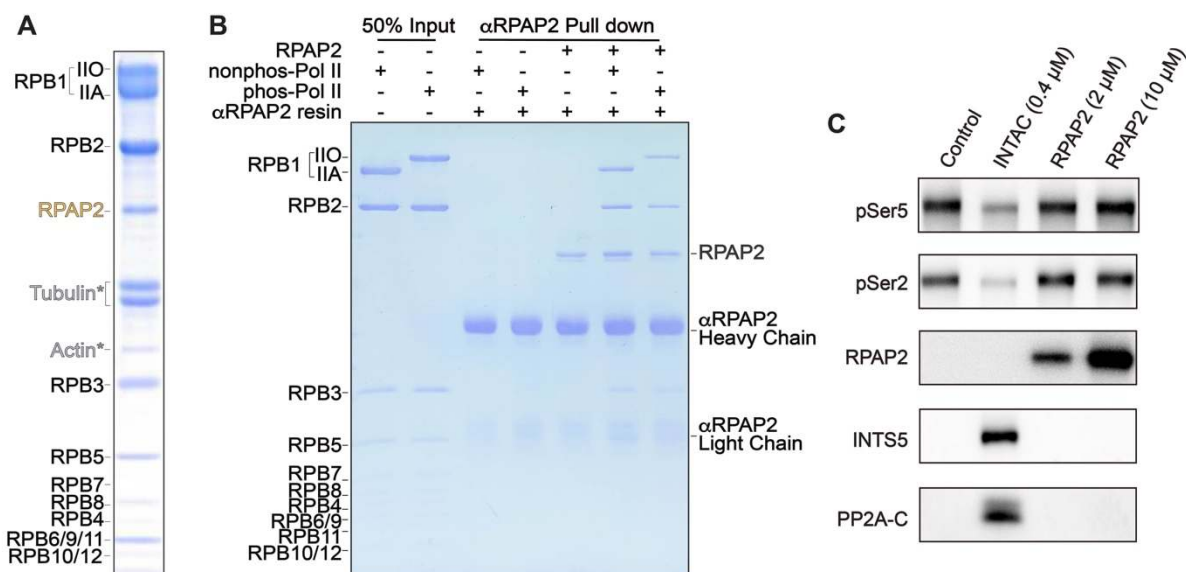
769 **ChIP-Rx and data analysis**

770 ChIP-Rx was conducted following previously described ([Orlando et al., 2014](#)). Raw reads
771 were trimmed by Trim Galore v0.6.6
772 (https://www.bioinformatics.babraham.ac.uk/projects/trim_galore/) to remove adaptors and
773 low-quality sequences (-q 25) and then aligned to the human genome hg19 assembly using
774 Bowtie2 v2.3.5.1 ([Amemiya et al., 2019](#)). PCR duplicates and low mapping quality reads
775 (MAPQ < 30) were removed using Picard tools v2.23.3 (<https://broadinstitute.github.io/picard/>)
776 (REMOVE_DUPLICATES = True) and SAMtools v1.9 ([Li et al., 2009](#)). Aligned read counts
777 were then normalized to Reads Per Million mapped reads (RPM) using deeptools v3.5.0
778 ([Ramirez et al., 2016](#)), and blacklist regions for hg19 genome annotation from ENCODE

779 project were removed ([Amemiya et al., 2019](#)). Reads aligned to human genome were
780 normalized based on $1e6/mm10_count$ calculated by SAMtools v1.9 ([Li et al., 2009](#)).
781 Normalized bigwig files were generated by deeptools v3.5.0 ([Ramirez et al., 2016](#)).

782 **Identification of transcription start sites**

783 To determine the genes expressed in DLD-1 cells, we used published PRO-cap bigwig
784 file for DLD-1 cells to determine the transcription start site (TSS) ([Aoi et al., 2020](#)). RefSeq
785 gene annotation was obtained from the UCSC Genome Browser and the transcription start sites
786 were defined as the maximum PRO-cap signal site at the region between TSS -10 bp and TSS
787 +300 bp. The transcript with maximum PRO-cap signal was selected as a representative gene
788 for those protein coding genes with multiple isoforms.

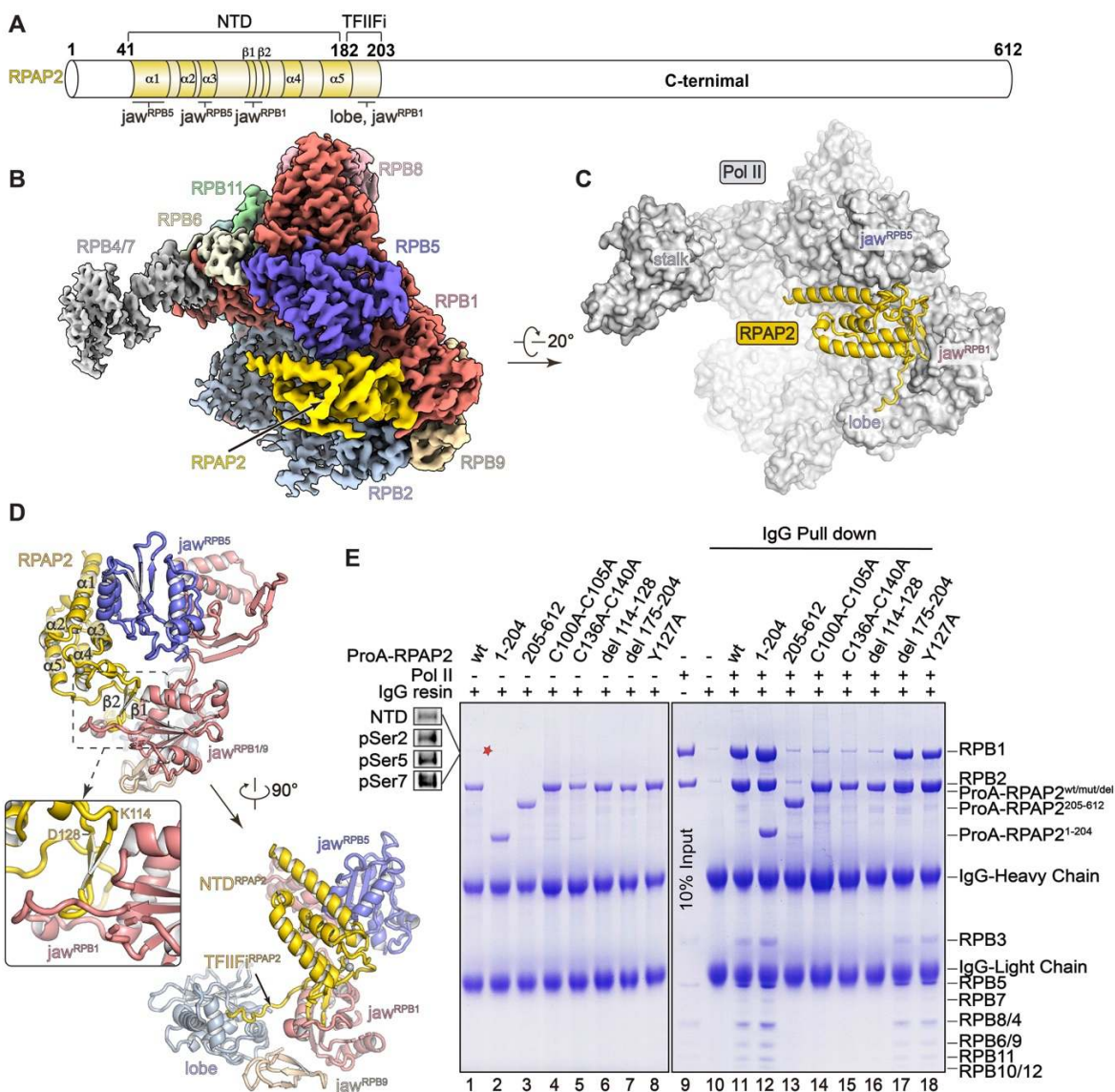


789

790 **Figure 1. Purification and characterization of RPAP2-Pol II complex.**

791 (A) Endogenous RPAP2 was co-purified during purification of human Pol II that was
 792 overexpressed in Expi293F cells. The purified complex was subjected to SDS-PAGE followed
 793 by Coomassie blue staining. Contaminating proteins were indicated with stars. The higher and
 794 lower band represent RPB1 in Pol Ilo and Pol Ila, respectively. (B) In vitro pulldown assay
 795 using unphosphorylated Pol II, phosphorylated Pol II and RPAP2. The bound proteins were
 796 subjected to SDS-PAGE followed by Coomassie blue staining. (C) In vitro phosphatase assay
 797 using purified RPAP2 and INTAC as enzymes and phosphorylated Pol II as substrate. The
 798 reactions were subjected to Western blotting using the indicated antibodies. The enzyme
 799 concentrations are indicated above each lane.

800 See also Figure S1.



801

802 **Figure 2. Overall structure of RPAP2-Pol II complex.**

803 (A) Domain structure of the RPAP2. The domains and regions built in structural model are
 804 colored and the unmodeled region is in white. Interfaces between RPAP2 and Pol II are
 805 indicated below.

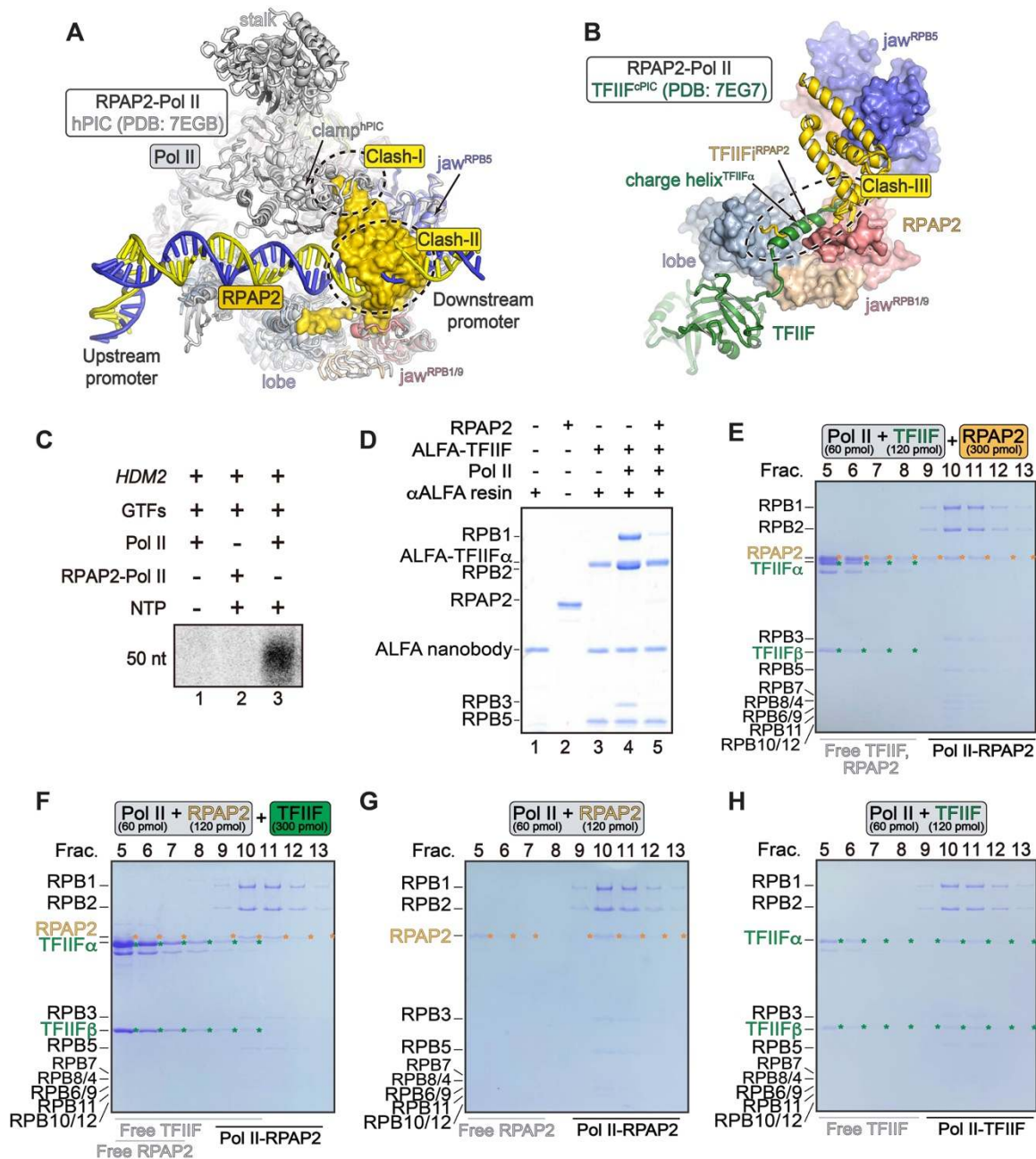
806 (B) A combined cryo-EM map of RPAP2-Pol II complex.

807 (C) Structural model of RPAP2-Pol II complex with Pol II shown in surface and RPAP2 shown
 808 in cartoon. The zinc cation at the zinc finger of RPAP2 is shown as a gray ball.

809 (D) Two views of intermolecular contacts between RPAP2 and Pol II. The interaction between
 810 the two-stranded β -sheet and RPB1 jaw is indicated with dashed box and shown in close-up
 811 view (middle panel).

812 (E) Interactions between Pol II and RPAP2. The cell lysates containing various Protein A
 813 (ProA)-tagged RPAP2 mutants or truncations were applied to IgG resins, which were further

814 incubated with purified Pol II. The unbound proteins were washed away and bound proteins
815 were subjected to SDS-PAGE followed by Coomassie blue staining. ProA-tagged RPAP2
816 overlaps with RPB2 in lanes 11-18 and the amounts of ProA-RPAP2 are indicated in lanes 1-
817 8. Note that trace amount of endogenous Pol II was pulled out by RPAP2^{WT} (lane 1).
818 See also Figure S2, S3 and Table S1.



819

820 **Figure 3. RPAP2 disrupts Pol II-TFIIF complex and inhibits PIC assembly.**

821 (A) Structures of RPAP2-Pol II and hPIC (PDB:7EGB) (Chen et al., 2021a) with Pol II
 822 superimposed. RPAP2-Pol II is colored as in Figure 2B and hPIC is colored in grey. The
 823 promoter is colored in yellow and blue for clarity. The GTFs of hPIC were omitted for
 824 complicity. RPAP2 is shown in surface representation. Steric clashes are indicated with dashed
 825 circle.

826 (B) Structural comparison of RPAP2-Pol II with core PIC (cPIC) (PDB: 7EG7) (Chen et al.,
 827 2021a) with Pol II superimposed. Pol II is shown in surface and steric clash between TFIIF

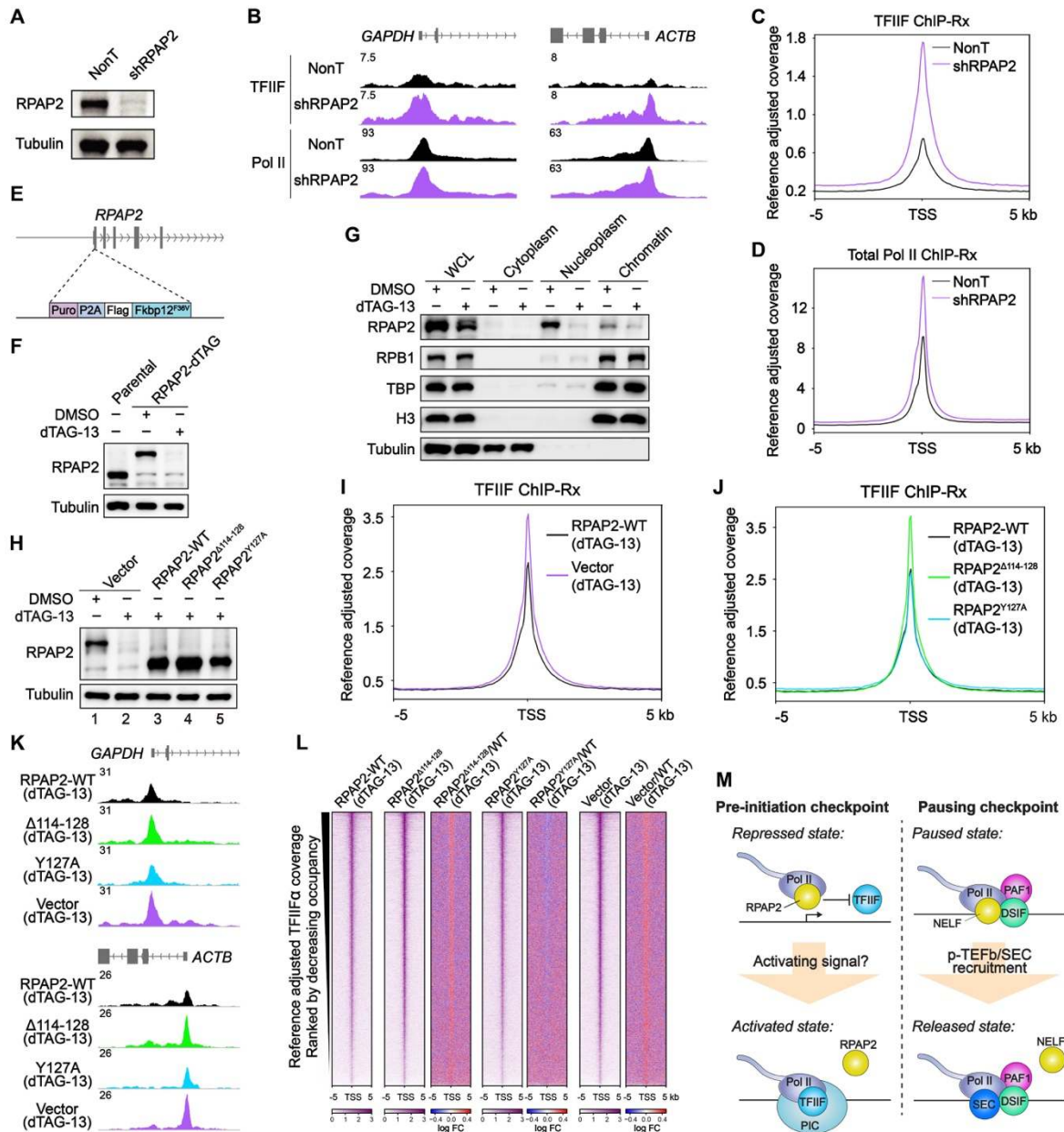
828 charge helix and TFIIF^{RPAP2} is indicated with dashed circle. Unnecessary regions of cPIC were
829 omitted for clarity.

830 **(C)** Autoradiogram of in vitro transcription initiation reactions. The complexes in the reactions
831 included purified GTFs (TFIIA, TFIIB, TFIID, TFIIF, TFIIE and TFIIH), *HDM2* promoter and
832 either Pol II or RPAP2-Pol II as indicated. As previously described ([Chen et al., 2021b](#)), the
833 reactions were incubated at 25°C for 30 min and then were subjected to urea polyacrylamide
834 gels and autoradiography.

835 **(D)** In vitro competitive binding assay using purified TFIIF (TFIIF α has an ALFA-tag), RPAP2
836 and Pol II. TFIIF and Pol II were pre-assembled and immobilized on anti-ALFA resins before
837 adding an equal amount of RPAP2. The bound proteins were subjected to SDS-PAGE and
838 stained using Coomassie blue.

839 **(E-H)** RPAP2 prohibits and disrupts Pol II-TFIIF interaction. RPAP2 (300 pmol) was
840 incubated with the pre-assembled Pol II-TFIIF (60 pmol) (E) or TFIIF (300 pmol) was
841 incubated with the pre-assembled RPAP2-Pol II (60 pmol) (F), followed by glycerol density
842 gradient ultracentrifugation. Fractions of glycerol density gradient centrifugation of RPAP2-
843 Pol II (G) and TFIIF-Pol II (H) are shown as control.

844 See also Figure S4.



845

846 **Figure 4. RPAP2 prohibits TFIIIF recruitment and cellular PIC assembly independently**
 847 **of the putative phosphatase activity.**

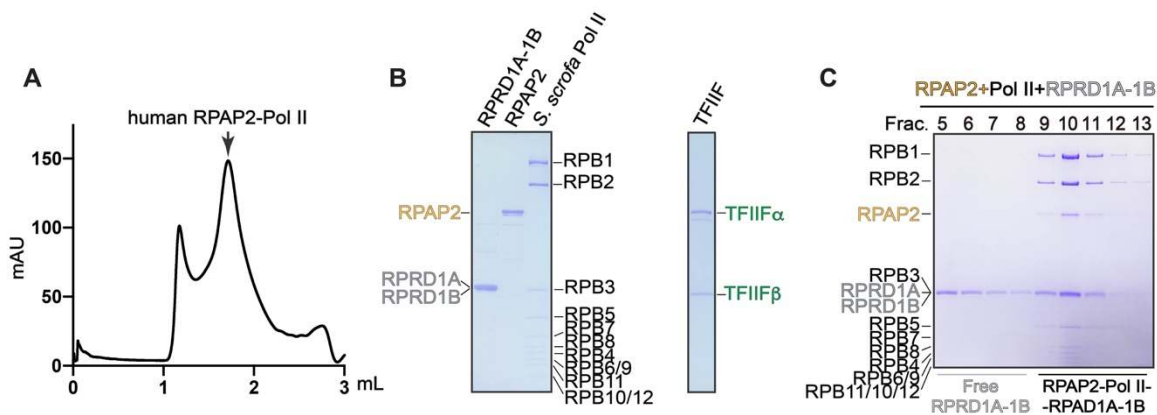
848 (A) Western blots of whole cell extracts from DLD-1 cells with knockdown of RPAP2 by
 849 shRNA.

850 (B) Representative track examples of genes *GAPDH* and *ACTB* showing the change of TFIIIF
 851 and Pol II occupancy by RPAP2 knockdown. Pol II occupancy is represented by its largest
 852 subunit RPB1.

853 (C and D) Metaplot showing the occupancy of TFIIIF (C) and total Pol II (D) measured by
 854 ChIP-Rx in NonT and RPAP2 knockdown cells.

855 (E) Schematic diagram of the generation of RPAP2-dTAG DLD-1 cells.

- 856 (F) Western blots of whole cell extracts RPAP2-dTAG or parental cells treated with DMSO or
857 dTAG for 3 hours.
- 858 (G) Subcellular fractionation of RPAP2-dTAG treated with DMSO or dTAG followed by
859 Western blotting. WCL, whole-cell lysate.
- 860 (H) Induced expression of wildtype RPAP2, RPAP2 $\Delta^{114-128}$, RPAP2 Y127A , or vector in RPAP2-
861 dTAG cells treated with dTAG-13, followed by Western of RPAP2.
- 862 (I) Metaplot showing the occupancy of TFIIF in dTAG treated RPAP2-dTAG cells with
863 induced expression of wildtype RPAP2 or vector.
- 864 (J) Metaplot showing the occupancy of TFIIF in dTAG treated RPAP2-dTAG cells with
865 induced expression of wildtype RPAP2, RPAP2 $\Delta^{114-128}$, or RPAP2 Y127A .
- 866 (K) Representative track examples showing TFIIF occupancy in dTAG treated RPAP2-dTAG
867 cells with induced expression of wildtype RPAP2, RPAP2 $\Delta^{114-128}$, RPAP2 Y127A , or vector.
- 868 (L) Heatmaps of TFIIF occupancy centered at TSS of promoters ranked by decreasing
869 occupancy.
- 870 (M) Proposed model of the pre-initiation checkpoint regulated by RPAP2 (left). Pausing
871 checkpoint (right) is shown for comparison.
- 872 See discussion for detailed description.
- 873



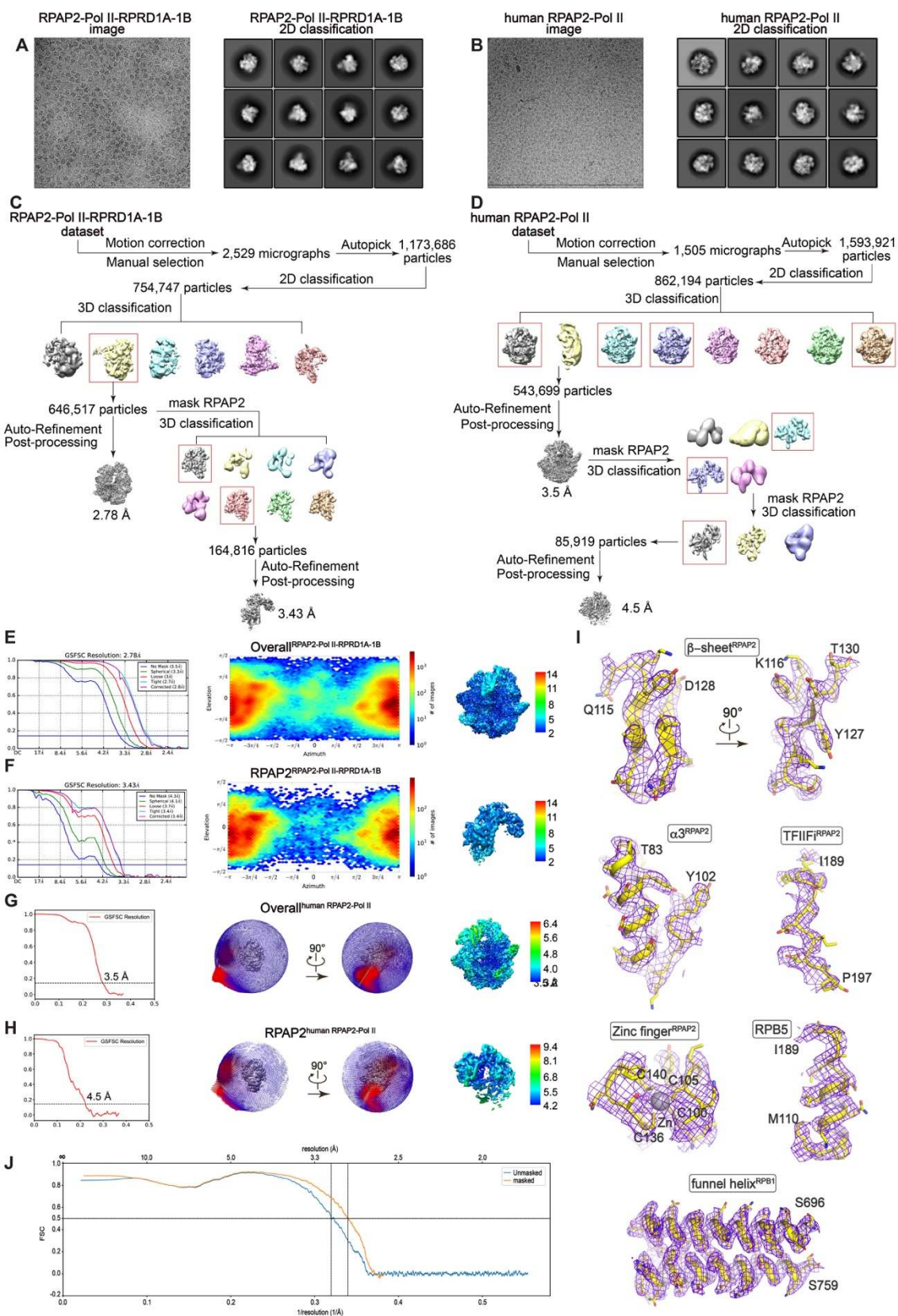
874

875 **Figure S1. Preparation of RPAP2-Pol II complexes, Related to Figure 1 and 2.**

876 (A) Size exclusion chromatogram of the purified human RPAP2-Pol II complex. Pol II was
877 overexpressed in Expi293F cells and endogenous RPAP2 was co-purified.

878 (B) Purified human RPRD1A-RPAD1B, RPAP2, TFIIF and *S. scrofa* Pol II (4 residues
879 substituted in *H. sapiens* Pol II) were subjected to SDS-PAGE and Coomassie blue staining.

880 (C) Fractions of glycerol density gradient centrifugation of RPAP2-Pol II-RPRD1A-RPAD1B
881 complex were subjected to SDS-PAGE followed by Coomassie blue staining.



882

883 **Figure S2. Structure determination and model building of RPAP2-Pol II complex,**

884 **Related to Figure 2.**

885 **(A and B)** Representative cryo-EM raw micrographs (left panels) and 2D classification (right
886 panels) of RPAP2-Pol II-RPRD1A-RPAD1B complex (A) and human RPAP2-Pol II complex
887 (B).

888 **(C and D)** Flow-charts of the cryo-EM image processing and 3D reconstruction for the
889 RPAP2-Pol II-RPRD1A-RPAD1B complex (C) and human RPAP2-Pol II complex (D).

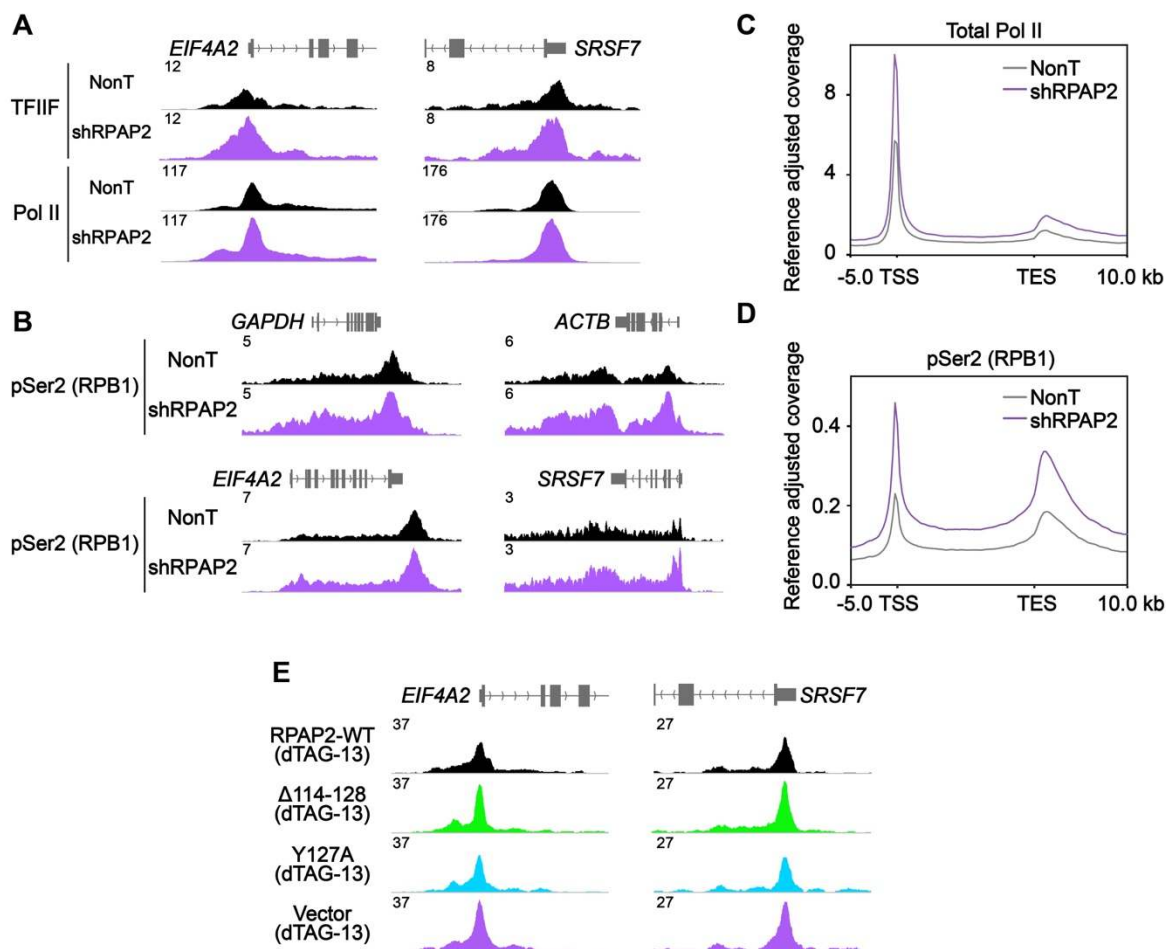
890 **(E-H)** The GSFSC curves, angular distributions, and local resolution estimation of the cryo-
891 EM reconstructions of RPAP2-Pol II-RPRD1A-RPAD1B complex (E and F) and human
892 RPAP2-Pol II complex (G and H).

893 **(I)** Representative structural models are shown with the corresponding cryo-EM maps shown
894 in mesh. Residues are shown in sticks, indicating that the model was correctly built.

895 **(J)** FSC curves between the model and cryo-EM map.

915 as indicated. The resins were extensively washed and subjected to SDS-PAGE and stained
916 using Coomassie blue.

917 **(D to H)** Position of RPAP2 on Pol II relative to other Pol II-binding proteins/complexes.
918 Structure of RPAP2-Pol II was superimposed with structures of PIC-MED (PDB:7ENA) ([Chen](#)
919 [et al., 2021b](#)) (C-F) and Pol II-Gdown1 (PDB: 6DRD) ([Jishage et al., 2018](#)) with Pol II shown
920 in gray surface. TFIIB (D), TFIIE (E), TFIIH (F), Mediator (G), Gdown1 (H) and RPAP2 are
921 shown as cartoon and the other GTFs were omitted for clarify. Structural comparison shows
922 no steric clash between RPAP2 and these complexes.



923

924 **Figure S5. The impact of RPAP2 knockdown or degradation on PIC assembly at**
925 **promoters, Related to Figure 4.**

926 (A) Representative track examples of genes *EIF4A2* and *SRSF7* showing the change of TFIIIF
927 and Pol II occupancy at promoters by RPAP2 knockdown. Pol II occupancy is represented by
928 its largest subunit RPB1.

929 (B) Representative track examples of genes *GAPDH*, *ACTB*, *EIF4A2* and *SRSF7* showing the
930 change of Pol II pSer2 occupancy at gene bodies by RPAP2 knockdown.

931 (C and D) Metaplot showing the occupancy of total Pol II (C) and pSer2 (D) at gene bodies
932 measured by ChIP-Rx in NonT and RPAP2 knockdown cells.

933 (E) Representative track examples of genes *EIF4A2* and *SRSF7* showing TFIIIF occupancy in
934 dTAG treated RPAP2-dTAG cells with induced expression of wildtype RPAP2, RPAP2 <sup>Δ 114-
935 128</sup>, RPAP2^{Y127A}, or vector.

936 **Table S1. Cryo-EM data collection, refinement and validation statistics, Related to**
 937 **Figure2.**

Complex	human RPAP2-Pol II		RPAP2-Pol II-RPRD1A-RPRD1B	
	overall	RPAP2	overall	RPAP2
Subcomplex				
EMDB				
PDB				
Data collection and processing				
Magnification	105,000	105,000	130,000	130,000
Voltage (kV)	300	300	300	300
Electron exposure (e-/Å ²)	~ 50	~ 50	~ 50	~ 50
Exposure rate (e-/pix/s)	~8	~8	~8	~8
Number of frames per movie	32	32	32	32
Automation software	SerialEM	SerialEM	SerialEM	SerialEM
Defocus range (µm)	-1.8 ~ -2.5	-1.8 ~ -2.5	-1.8 ~ -2.5	-1.8 ~ -2.5
Pixel size (Å)	1.356	1.356	1.044	1.044
Symmetry imposed	C1	C1	C1	C1
Micrographs (no.)	1,505	1,505	2,529	2,529
Total of extracted particles (no.)	1,593,921	1,593,921	1,173,686	1,173,686
Total of refined particles (no.)	543,699	85,919	646,517	164,816
Local resolution range (Å)	3.2-6.4	4.2-9.4	2.0-14.0	2.0-14.0
Resolution Masked 0.143 FSC (Å)	3.5	4.5	2.8	3.4
Refinement				
Map sharpening B-factor (Å ²)	-155.1	-207.1	-120.5	-101.6
Initial model used (PDB code)			7EGB, 4FC8	
Refinement package			Phenix (real space)	
r.m.s. deviations				
Bond lengths (Å)			0.017	
Bond angles (°)			1.078	
Validation				
MolProbity score			2.2	
All-atom clashscore			14.89	
Rotamers outliers (%)			0.62	
Cβoutliers (%)			0	
CaBLAM outliers (%)			3.82	
B-factors (min/max/mean)				
Protein			29.18/299.23/93	
			.05	

Ligand	54.80/186.58/11
	2.49
Overall correlation coefficients	
CC (mask)	0.81
CC (peaks)	0.68
CC (volume)	0.8
Ramachandran plot statistics	
Favored (%)	90.84
Allowed (%)	8.79
Disallowed (%)	0.38

938

939

940 **Video S1. Overall structure of RPAP2-Pol II complex, Related to Figure2.**

941 The composite cryo-EM map and structural model of RPAP2-Pol II.

942

943 **Video S2. Steric clash between TFIIF and RPAP2, Related to Figure3.**

944 Structural comparison of RPAP2-Pol II with core PIC (cPIC) (PDB: 7EG7) ([Chen et al., 2021a](#))

945 with Pol II superimposed. Pol II is shown in surface and steric clash between TFIIF charge

946 helix and TFIIF^{RPAP2} is indicated with white circle. Unnecessary regions of cPIC were omitted

947 for clarity.